(2)

TECHNICAL REPORT BRL-TR-3181

BRL

THE MECHANICAL RESPONSE OF M30, XM39, AND JA2 PROPELLANTS AT STRAIN RATES FROM 10^{-2} TO 250 SEC^{-1}

GEORGE A. GAZONAS

JANUARY 1991

U.S. ARMY LABORATORY COMMAND

BALLISTIC RESEARCH LABORATORY
ABERDEEN PROVING GROUND, MARYLAND

NOTICES

Destroy this report when it is no longer needed. DO NOT return it to the originator.

Additional copies of this report may be obtained from the National Technical Information Service, U.S. Department of Commerce, 5285 Port Royal Road, Springfield, VA 22161.

The findings of this report are not to be construed as an official Department of the Army position, unless so designated by other authorized documents.

The use of trade names or manufacturers' names in this report does not constitute indorsement of any commercial product.

REPORT DOCUMENTATION PAGE

Form Approved
OMB No. 0704-0188

1. AGENCY USE ONLY (Leave blank)	2. REPORT DATE	3. REPORT TYPE AND DATES COVERED
	January 1991	Final, Sep 89 - Feb 90

4. TITLE AND SUBTITLE

The Mechanical Response of M30, XM39, and JA2 Propellants at Strain Rates from 10^{-2} to 250 Sec^{-1}

5. FUNDING NUMBERS

PR: 1L161102AH43

6. AUTHOR(S)

George A. Gazonas

7. PERFORMING ORGANIZATION NAME(S) AND ADDRESS(ES)

8. PERFORMING ORGANIZATION REPORT NUMBER

9. SPONSORING/MONITORING AGENCY NAME(S) AND ADDRESS(ES)

US Army Ballistic Research Laboratory
ATTN: SLCBR-DD-T
Aberdeen Proving Ground, MD 21005-5066

10. SPONSORING/MONITORING AGENCY REPORT NUMBER

BRL-TR-3181

11. SUPPLEMENTARY NOTES

12a. DISTRIBUTION/AVAILABILITY STATEMENT

Approved for public release; distribution unlimited.

12b. DISTRIBUTION CODE

13. ABSTRACT (Maximum 200 words)

The mechanical response of M30, XM39, and JA2 gun propellants at strain rates from 10^{-2} to 250 sec^{-1} is characterized using the BRL's new Hi-Rate Servohydraulic test apparatus. At axial strain rates of 250 sec^{-1}, there is good experimental agreement between the compressive moduli determined on the Drop Weight and Servohydraulic apparatuses, yet the post-yield responses vary because of differing displacement history inputs. All three propellants deformed in a ductile fashion and sustained over 40% shortening. The M30 and XM39 propellants deformed by macroscopic fracture and work-softened after reaching maximum stress. The JA2 propellant deformed by macroscopic flow and work-hardened throughout the deformation history. The absorbed strain energy density per unit volume at 30% shortening and strain rate of 250 sec^{-1} is 16 and 23 MPa for the XM39 and M30 propellants, respectively. In contrast, the absorbed strain energy density for the JA2 propellant is only 8 MPa and is due to the relatively low flow stress sustained by the material during deformation. A viscoelastic characterization reveals that the secant and relaxation moduli for these propellants can be represented by a power law in time with nonlinear behavior in the time range from 10^{-2} to 10^{+4} milliseconds.

14. SUBJECT TERMS	15. NUMBER OF PAGES
Gun Propellants, High Rate Testing, Mechanical Properties, Viscoelasticity, Servohydraulic Test Apparatus, Strain Energy Density	49
	16. PRICE CODE

17. SECURITY CLASSIFICATION OF REPORT	18. SECURITY CLASSIFICATION OF THIS PAGE	19. SECURITY CLASSIFICATION OF ABSTRACT	20. LIMITATION OF ABSTRACT
UNCLASSIFIED	UNCLASSIFIED	UNCLASSIFIED	SAR

INTENTIONALLY LEFT BLANK.

TABLE OF CONTENTS

LIST OF FIGURES

LIST OF FIGURES (continued)

LIST OF TABLES

1. INTRODUCTION

The mechanical response of gun propellant is of interest to interior ballisticians since fracture damage can adversely affect the mass generation rate during the ballistic cycle. Three macroscopic fracture mechanisms have been identified which include: 1) perforation rupture (hydraulic fracturing), 2) direct grain impact, and 3) intergranular contact stress[1]. To the author's knowledge, the phenomenon of perforation rupture in gun propellant has not been experimentally investigated by interior ballisticians although hydraulic fracture studies are common in the rock mechanics literature[2]. Interior ballisticians have investigated fracture by direct grain impact using a Gas Gun Impact Tester[3] (GGIT), Drop Weight Mechanical Properties Tester[4] (DWMPT), Split Hopkinson Bar Apparatus[5] (SHB), and most recently a new High Rate MTS Systems Corporation Servohydraulic Tester (MTS) which will be discussed in more detail later. Intergranular contact stress fracture phenomena have been investigated with a variety of bed testers[6,7,8] and are primarily devoted to evaluating the bulk response of the propellant bed.

The pressure, temperature, and strain history induced in a propellant bed during ignition and combustion can be severe and complex; x-ray methods[9,10] and in situ pressure pulse monitoring methods[11] provide estimates of operational strain rates that approach 10^4 sec^{-1} and peak pressures that approach 700 MPa[12]. Operating temperatures will vary with climate and typically range from -46° to 63° Celsius. Over this temperature range, a brittle-ductile transition in propellant response might be observed as in many materials whose deformation mechanisms are thermally activated.

One objective of propellant testing programs is to relate single grain mechanical property data such as compressive modulus, absorbed strain energy density, yield stress or strain, et cetera, to the combustion characteristics (primarily the mass generation rate) of the deformed propellant. The studies aim to determine if fracture generated surface area is responsible for catastrophic failure and breech-blow phenomena that sometimes occur during gun firing. Characterization of a material's mechanical response might also aid in survivability studies of armored weapons systems which are vulnerable to various forms of attack. An ancillary experimental objective is to provide material property data for use in numerical hydrodynamic simulations of the ballistic process.

This report describes the mechanical property test results obtained for the room temperature, uniaxial compressive deformation of M30, XM39 and JA2 gun propellants at strain rates from 10^{-2} to 250 per second using the Ballistic Research Laboratory's new servohydraulic mechanical properties tester. Also included are comparisons with data obtained on the Split Hopkinson Bar Apparatus and Drop Weight Mechanical Properties Tester. Finally, a preliminary viscoelastic characterization of the gun propellant provides relaxation moduli, secant moduli, and a test for "material" linearity/nonlinearity.

2. SERVOHYDRAULIC APPARATUS AND DATA ACQUISITION

The High Rate MTS 810 Material Test System (Figure 1) consists of a conventional two-pole press with a servohydraulically actuated ram that operates from quasistatic velocities to a maximum velocity which approaches 12 m/sec; the maximum velocity imparts a maximum strain rate of 1200 sec^{-1} on a 10 mm long specimen. Other essential components include a bell and cone piston assembly which permit fixed amounts of total specimen strain, a lower N_2-spring piston designed to absorb the impact shock, a 60 kN Kistler force gage mounted in the upper moving piston, and an externally mounted LVDT for displacement measurement. A Thermotron conditioning oven/refrigerator surrounds both upper and lower pistons and permits temperature testing from -85° to 90° Celsius. Arbitrary load and/or displacement histories can be imparted to the specimen by computer control. Raw force and displacement data are acquired, stored, and then analyzed with a Norland 3001 data acquisition system. Finally, plots of stress and strain versus time, and stress versus strain are printed on a Dataproducts dot matrix printer via RS232 port. The data can also be uploaded via RS232 port

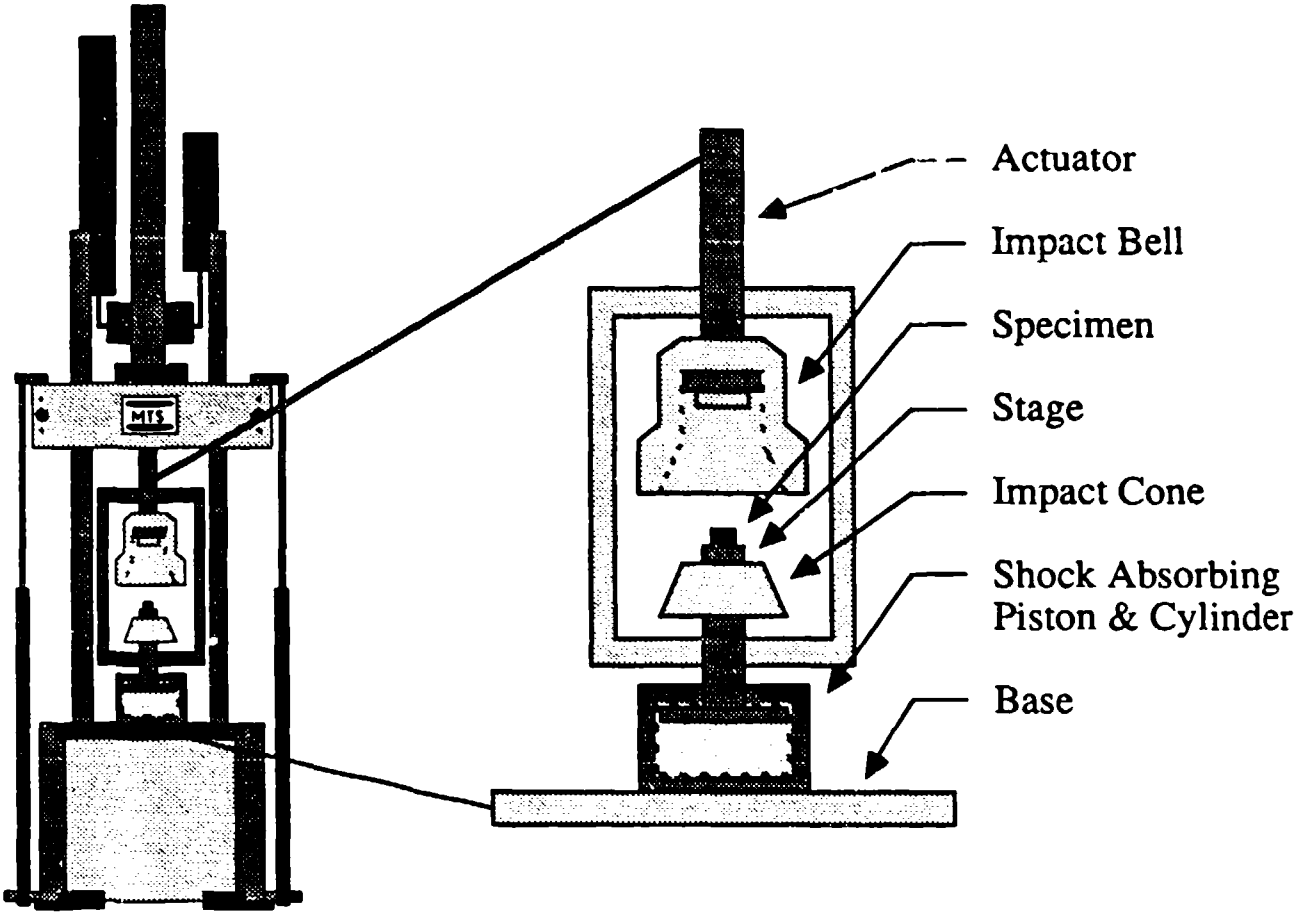

Figure 1. Servohydraulic Test Apparatus with Upper Bell and Impact Cone Piston Assembly.

to a PC and converted to ASCII format for more sophisticated analysis.

The 60 kN Kistler force gage is calibrated every 2 to 3 months using a Morehouse Ring Dynamometer (S/N M-4644); the instrument is certified by the National Bureau of Standards to have an uncertainty to within .003 percent of the applied load. The maximum uncertainty in force measurement is 2 percent and is determined by comparing the force readings from the Dynamometer with the amplified signal on the Norland data acquisition system. The uncertainty in the displacement measurement is within 1 percent as determined by comparison with a National Bureau of Standards certified displacement dial gage (personal communication with Aaron Anderson, MTS Project Engineer).

2.1 Apparatus Stiffness. A mechanical idealization of the deformation apparatus (Figure 2) assumes that all machine components are linearly elastic. Contact nonlinearities due to interface mismatch are disregarded. The apparatus idealization consists of three spring components in series. K_{mu} represents the upper machine stiffness and consists of stiffness contributions from the upper piston, the actuator, the hydraulic fluid, the crosshead and tie rods. K_s represents the specimen stiffness. K_{ml} represents the lower machine stiffness and consists of stiffness contributions from the lower piston, the N_2-filled pressure vessel, and the load unit base. The force is assumed to be the same in each spring, however the displacements in each spring will vary according to their individual stiffnesses.

In a typical test, the measured displacement, d, must be corrected for stiffnesses K_{mu} and K_{ml} in order to accurately calculate the displacements in the specimen. Fortunately, gun propellants are relatively soft in comparison to the apparatus so that the correction is not very large. We can lump

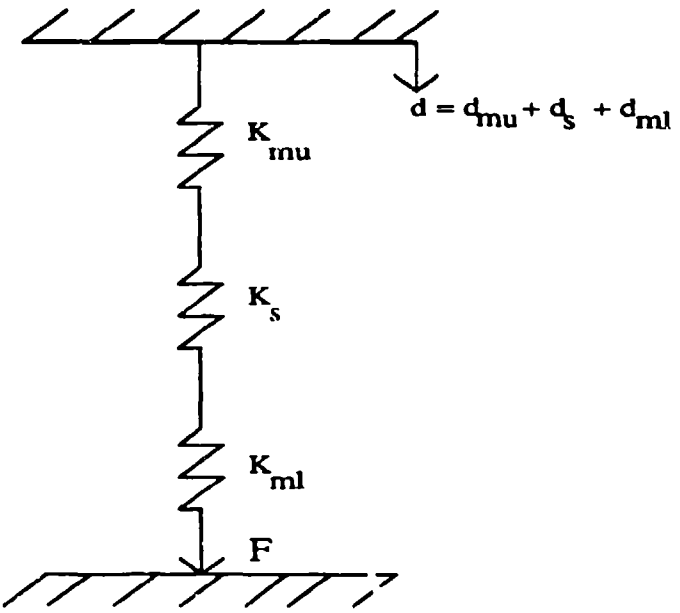

Figure 2. Mechanical Idealization of the MTS using a Linear Elastic Spring Model.

together the K_{mu} and K_{ml} stiffness contributions and arrive at an apparatus stiffness K_a according to the equation:

$$1/K_a = 1/K_{mu} + 1/K_{ml} \quad (1)$$

where the total system stiffness K is given by:

$$K = 1/(1/K_a + 1/K_s) = F/d \quad (2)$$

where

F = total measured force
d = total measured displacement

The apparatus stiffness is determined by performing an experiment using a specimen whose stiffness K_s is very large and hence negligible relative to the ratio $1/K_a$. A set of seven experiments was conducted using a hardened steel slug and the average apparatus stiffness was determined to be $K_a = 91.87 \pm 4.8$ kN/mm.

2.2 Stored Elastic Strain Energy. The amount of elastic strain energy, W, stored in a cylindrical elastic rod under applied force, F, is given by:

$$W = F^2/2K \quad (3)$$

where the stiffness, K, is given by:

$$K = AE/L \quad (4)$$

where

L = rod length
A = rod area
E = Young's modulus

We can determine how the elastic strain energy, W, is partitioned between the apparatus and a propellant grain during compression by first determining a "typical" propellant grain stiffness. The stiffness of a grain of XM39 at 250 sec^{-1} with crossectional area, A = 24.5 mm^2, length, L = 6.5 mm, and compressive modulus, E = 3.5 GPa, is K = 13 kN/mm. At a strain rate of 250 sec^{-1}, XM39 yields at about 47 MPa or an axial force, F = 1.15 kN. Hence from Equation 3 the elastic energy stored within the grain at yield is .051 kN-mm. Using the apparatus stiffness and Equation 3 we see that the energy stored in the apparatus at yield is .0072 kN-mm which is 7 times less than the elastic strain energy stored in the specimen, or only 12 percent of the total system elastic strain energy.

This observation has important consequences for studying the post-failure response of gun propellant since in stiff testing machines the elastic strain energy present in the apparatus is negligible relative to the specimen and failure of the specimen can proceed under stable conditions. Jaeger and Cook[2] regard the failure process as being stable if the post-failure material stiffness is less than that of the apparatus. Under these conditions the complete stress-strain curve can be cap-

tured. However, in soft testing machines the elastic strain energy stored in the apparatus is violently released during specimen failure and hence the complete post-failure response of the specimen cannot be obtained.

Specimen failure for brittle materials is defined[2] in the classical macroscopic sense as a continuous process that begins at the maximum stress (point where the tangent modulus of the stress-strain curve is zero) and continues for an indefinite period (tangent modulus of the stress-strain curve is negative) until ultimate failure or the complete loss of load bearing capacity occurs (Figure 3). If ultimate failure occurs at relatively small strains the material is termed brittle. Ductile materials ultimately fail at relatively large strains and can be accompanied by significant workhardening behavior. It is important for interior ballisticians to be able to identify when a particular propellant begins to fracture, since it is at this time that additional surface area becomes available for burning. However, by examining stress versus strain curves alone, no information can be obtained regarding the mechanism of deformation whether it be fracture, compaction, crystal plastic flow, bond stretching,

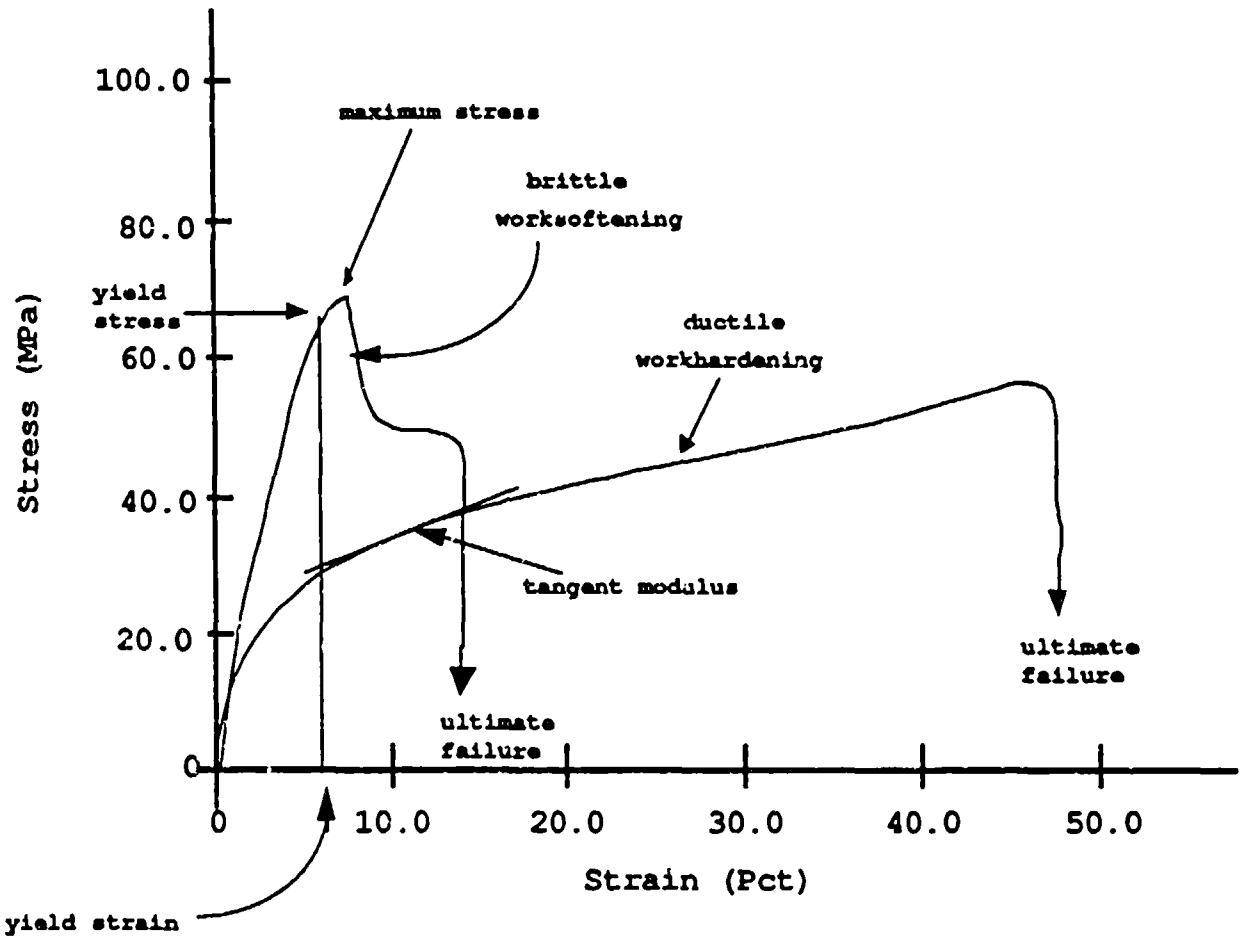

Figure 3. Macroscopic Brittle-Ductile Response for Materials.

et cetera, or how the relative contributions of the mechanisms are partitioned in pressure, temperature, and strain space. Deformation by fracture can be identified by detailed micromechanical observation, using, for example, the scanning electron microscope or optical microscope. Once fracture has been identified as a dominant deformation mechanism for a particular propellant then an important experiment would be to perform a series of tests where different specimens are deformed to increasing amounts of fixed total strain at various strain rates and temperatures; the new servohydraulic test apparatus has this capability because of its unique bell and cone impact housing design. The deformed grains could then be burned in a mini-closed bomb[1] and the combustion characteristics (burning rate, mass generation rate, et cetera) could be quantitatively related to one or more gross mechanical property parameters. Research is presently under way to investigate the effects of strain rate, temperature, and degree of fixed axial strain on the mass generation rate and burning rate of M30 and JA2 propellants.

3. EXPERIMENTAL PROCEDURE

Right circular cylinders of M30, XM39, and JA2 (abbreviated lots are 67878, 1333, and S110 respectively) are cut from granular propellant stock using an Isomet diamond saw. Care is taken to cut the ends parallel to each other and perpendicular to the cylinder axis so that the compressive deformation is coaxial and uniform. Specimen dimensions are measured with a vernier caliper and length to diameter ratios (L/D) average about 1:1 (Table 1) for each of the propellant formulations[13] (Table 2).

Table 1. Average Lengths, Diameters, and Perforation Diameters of Propellant Specimens.

	Length (mm)	Diameter (mm)	L/D	Perf.-Diam. (mm)
M30	9.581 ± 0.34	7.042 ± 0.059	1.361	.686
XM39	6.929 ± 0.37	5.643 ± 0.046	1.228	.305
JA2	9.091 ± 0.43	8.719 ± 0.068	1.043	.483

Table 2. Percent Composition of JA2, M30, and XM39 Gun Propellants.

Propellant	JA2	M30		XM39
Component	%	%	Component	%
Nitrocellulose	59.0	28.0	RDX (ground)	76.0
NC Nitration Level	13.0	12.6	Cell. Acetate Butyrate	12.0
Nitroglycerin	15.0	22.0	Acetyl Triethyl Citrate	7.6
Nitroguanidine	0.0	48.0	Nitrocellulose	4.0
Ethyl Centralite	0.0	2.0	NC Nitration Level	12.6
Diethylene Glycol			Ethyl Centralite	0.4
Dinitrate	25.0	0.0		
Akardit II	1.0	0.0		

All tests are performed at ambient pressure (0.1 MPa) and temperature (22° Celsius). Molybdenum disulphide, MoS_2, is applied sparingly to the specimen ends prior to testing in order to reduce frictional end effects and specimen barreling. A minimum of five specimens are deformed to 50 percent strain, at nominal strain rates of .01, 1, 100, and 250 per second.

3.1 Data Reduction. The raw force and displacement data are reduced and converted to stress versus strain plots as previously reported[13]. Two additions to the standard data reduction program include an apparatus distortion correction and an algorithm for automatically picking the yield stress. The net axial stress is determined using the initial cross-sectional area of the specimen minus the perforation area. In future work, a stress correction due to increasing crossectional area of the specimen can be made after the Poisson's ratio is determined using a lateral deformation gage. The raw force and displacement voltages versus time, stress and strain versus time, calibration factors, specimen dimensions, and the following mechanical parameters are calculated and stored on floppy disks: maximum stress, stress and strain at yield, strain rate, compressive modulus, strain energy density absorbed per unit volume at yield, strain energy density at selected strain increments past yield, ratios of subsequent strain energy density values relative to the strain energy density at yield. Macroscopic yield is defined[5,13] as the stress level where the material most rapidly loses its ability to sustain load; the yield stress level is determined by finding the minimum in the second derivative of stress with respect to time. Since the second derivative data is somewhat noisy, an n-point smoothing algorithm is used so that a consistent, operator-independent criterion exists for picking the minimum. Equally arbitrary definitions of the yield point, such as the proportional limit definition (stress level at the end of the linear range) or offset method definition (stress level after 0.2 percent offset strain), were not viable candidates since for the former definition a suitable linear range is difficult to determine for these materials and for the latter definition the yield would occur at fractions of a percent of maximum stress and the strain dependence of yield could not be investigated. The choice of the yield point, as it relates to strength loss due to fracture, should ultimately be constrained by microphysical considerations.

3.2 Grain Geometry Effects. Each of the propellant grains contains seven perforations so that during axial compression a highly inhomogeneous stress field could develop due to internal stress concentrations and noncoaxiality of the perforations with the grain axis. The results of this study provide data regarding the mechanical or structural response of propellant grains which are useful for evaluating how grains might behave during axial impact in a gun cartridge. In order to determine material or constitutive properties of gun propellant, for use in numerical simulations of the ballistic process, tests on solid propellant grains could be performed in order to ensure homogeneity of the stress field within the specimen. The determination of material properties is necessary in order to predict the location and intensity of pressure instabilities due to fracturing in a propellant bed. A future study is planned to evaluate the degree to which the propellant response is affected by grain geometry. This will include a study of the propellant response by varying the length to diameter ratio, solid versus perforated grains, lubricated versus unlubricated end conditions, multiaxial stress states including compression, tension and possibly torsion.

4. EXPERIMENTAL RESULTS

Summaries of the experimental results for the uniaxial compression of M30, XM39 and JA2 as a function of strain rate appear in Tables 3,4,and 5 respectively. Synoptic plots of axial stress versus strain as a function of strain rate, reveal that M30 and XM39 reach a maximum stress and then work-soften in response to a constant strain rate input (Appendix A). JA2 responds by continually work-hardening throughout its deformation history. All three propellants behave in a macroscopically ductile fashion and sustained over 40 percent axial shortening.

Table 3. JA2 Servohydraulic Compression Test Results. Y is the Yield Point and is defined as the Stress Level Which Corresponds to the Minimum in the Second Derivative of Stress with Respect to Time.

	Nominal Strain Rate (sec^{-1})		
	10^{-2}	1	100
Max. Stress (MPa)	22.65 ± 1.30	37.75 ± 6.35	61.69 ± 2.62
Stress @ Y (MPa)	4.49 ± 0.64	9.26 ± 1.73	14.45 ± 1.58
Strain @ Y (%)	3.48 ± 0.75	3.25 ± 0.59	3.06 ± 0.37
Strain Rate (sec^{-1})	.0098 ± .001	0.97 ± 0.04	92.06 ±15.27
Modulus (GPa)	0.19 ± 0.03	0.41 ± 0.11	0.77 ± 0.19
Energy @ Y (MPa)	0.06 ± 0.02	0.12 ± 0.05	0.15 ± 0.02
	200	250	
Max. Stress (MPa)	77.96 ±11.81	72.29 ± 9.26	
Stress @ Y (MPa)	18.30 ± 1.38	17.30 ± 1.50	
Strain @ Y (%)	3.05 ± 0.84	3.23 ± 0.63	
Strain Rate (sec^{-1})	200.30 ± 8.21	244.50 ± 3.32	
Modulus (GPa)	0.77 ± 0.08	0.79 ± 0.09	
Energy @ Y (MPa)	0.24 ± 0.07	0.21 ± 0.05	

Table 4. M30 Servohydraulic Compression Test Results.

	Nominal Strain Rate (sec^{-1})			
	10^{-2}	1	100	250
Max. Stress (MPa)	41.07 ±28.82	51.41 ± 2.78	94.55 ± 2.86	105.44 ± 2.45
Stress @ Y (MPa)	28.82 ± 3.91	43.25 ± 3.21	60.77 ± 4.77	75.50 ±11.44
Strain @ Y (%)	4.37 ± 1.45	5.08 ± 2.07	4.55 ± 0.30	3.65 ± 0.81
Strain Rate (sec^{-1})	.0096 ± 0.001	0.96 ± 0.03	118.20 ±13.32	240.50 ± 5.65
Modulus (GPa)	1.21 ± 0.40	1.51 ± 0.57	2.34 ± 0.24	2.76 ± 0.22
Energy @ Y (MPa)	0.43 ± 0.25	0.86 ± 0.44	0.80 ± 0.12	1.18 ± 0.59

Table 5. XM39 Servohydraulic Compression Test Results.

	Nominal Strain Rate (sec^{-1})			
	10^{-2}	$4x10^{-2}$	1	100
Max. Stress (MPa)	28.26 ± 0.85	28.89 ± 0.61	39.65 ± 1.79	71.51 ± 2.18
Stress @ Y (MPa)	14.68 ± 1.27	18.84 ± 2.123	5.93 ± 2.60	55.93 ± 3.73
Strain @ Y (%)	2.77 ± 0.98	2.86 ± 0.56	3.66 ± 0.53	3.52 ± 0.22
Strain Rate (sec^{-1})	0.01 ± 0.0002	0.04 ± 0.0003	0.97 ± 0.02	104.60 ± 3.31
Modulus (GPa)	1.13 ± 0.35	1.08 ± 0.09	1.73 ± 0.04	2.98 ± 0.78
Energy @ Y (MPa)	0.12 ± 0.04	0.17 ± 0.07	0.49 ± 0.10	0.57 ± 0.17

	250
Max. Stress (MPa)	65.91 ± 7.92
Stress @ Y (MPa)	49.82 ±15.06
Strain @ Y (%)	3.26 ± 1.92
Strain Rate (sec^{-1})	246.10 ± 8.50
Modulus (GPa)	3.07 ± 1.27
Energy @ Y (MPa)	0.37 ± 0.13

The compressive modulus (Figure 4) and the yield stress (Figure 5) both increase as a function of strain rate for all three propellants, yet the strain at yield remains relatively constant (Figure 6). Note that even though the moduli of M30 and XM39 are nearly identical, the strain energy density, τ, absorbed at yield by the M30 propellant, is 2 and 5 times greater than that of XM39 and JA2 respectively (Figure 7). This observation could have important consequences for the design of new fracture resistant propellants as it appears that the triple base M30 propellant has higher yield stress levels than either the double base JA2 or single base XM39 propellants. However, visual inspection of deformed specimens of M30 and XM39 propellant reveals that macroscopic fractures develop in specimens tested at all strain rates above 10^{-2} sec^{-1}; none of the JA2 specimens macroscopically fractured at any of the strain rates tested. Furthermore, rapid snapshots taken at 10 frames per second during the axial compression of specimens of XM39 reveal that macroscopic fractures begin to develop after about 2 seconds, or at 28 MPa and 7.7 percent axial strain. However, the stress and strain at yield determined using the minimum second derivative of stress with respect to time criterion indicates that the yield stress and strain occur at only 18.8 Mpa and 2.9 percent respectively (Table 5). Since the appearance of macroscopic fractures does not correspond with macroscopic yield of the specimen, detailed microscopic observations are needed to define when microfracturing begins.

The average compressive moduli of M30, XM39, and JA2 at room temperature and a strain rate of 250 sec^{-1}, determined using the Servohydraulic Tester, compare well with the moduli determined using the Drop Weight Mechanical Properties Tester (Table 6). However, the stress versus strain responses considerably differ, particularly in the post-failure region for the work-softening M30 and XM39 propellants (Figures 8a and 8b). The difference in material response is attributed to the differing input strain histories between the devices. The input strain rate on the MTS is computer controlled and remains relatively constant throughout the deformation history. However, the strain rate on the DWMPT remains constant only to yield, then becomes zero, negative, and begins to increase again as the upper load piston rebounds off the specimen preparing for a second impact. Multiple ram impacts will reoccur until the total kinetic energy of the ram is dissipated in work done in deforming the propellant, and frictional and impact sound losses. Figure 8c illustrates a typical multiple impact response for JA2. Since the response is ductile, the post-yield stress-strain curves compare more favorably with that of the MTS since instabilities present during macroscopic failure are not present.

Table 6. A Comparison of Compressive Moduli Determined Using the MTS and DWMPT at Room Temperature and Strain Rate of 250 sec^{-1}.

	M30	XM39	JA2
DWMPT Modulus (GPa)	2.74	4.08	.782
MTS Modulus (GPa)	2.76	3.07	.790

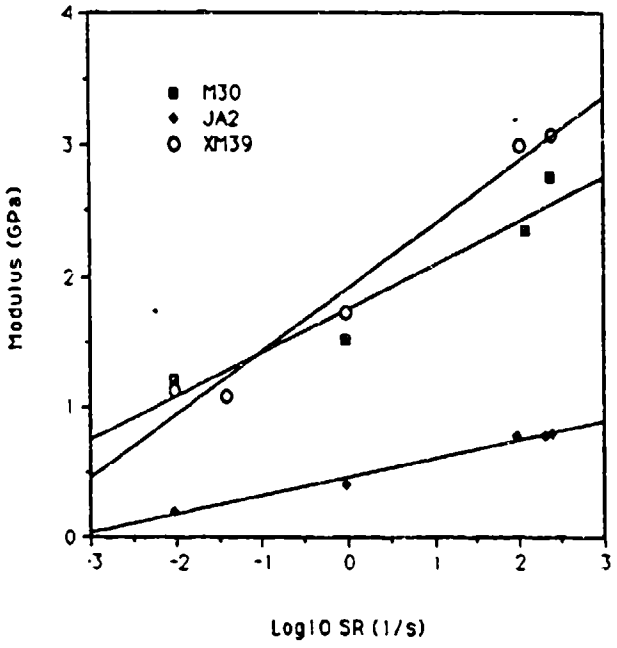

Figure 4. Modulus versus Strain Rate.

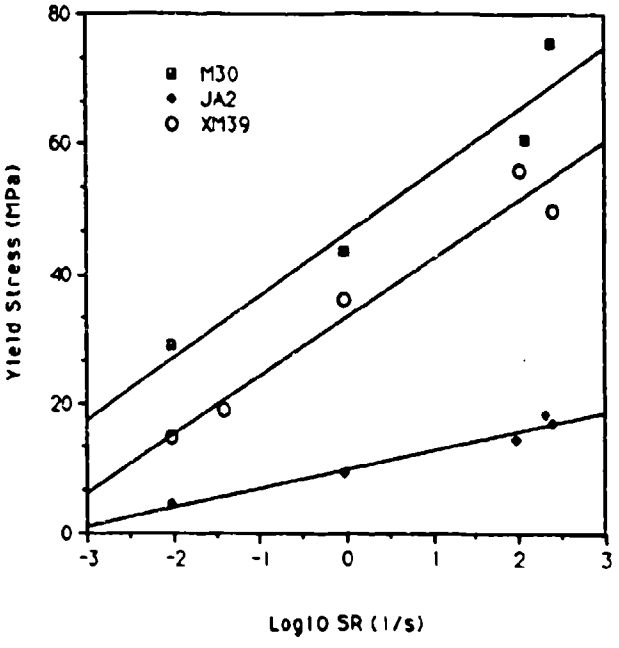

Figure 5. Yield Stress versus Strain Rate.

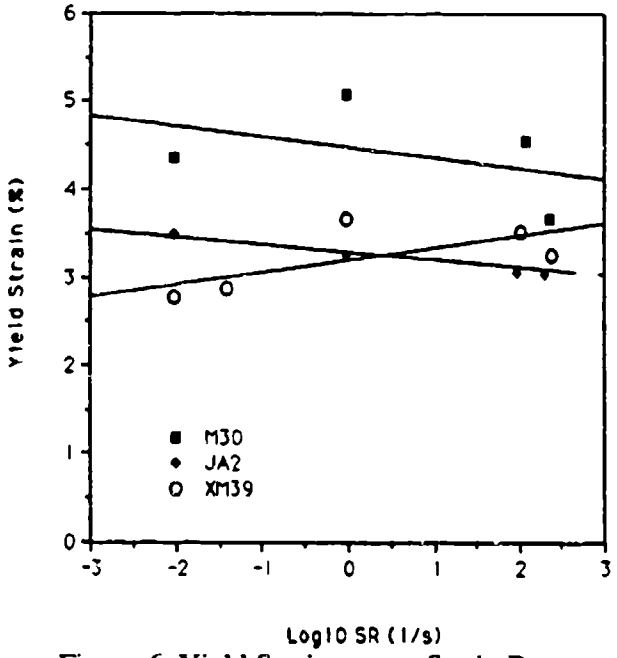

Figure 6. Yield Strain versus Strain Rate.

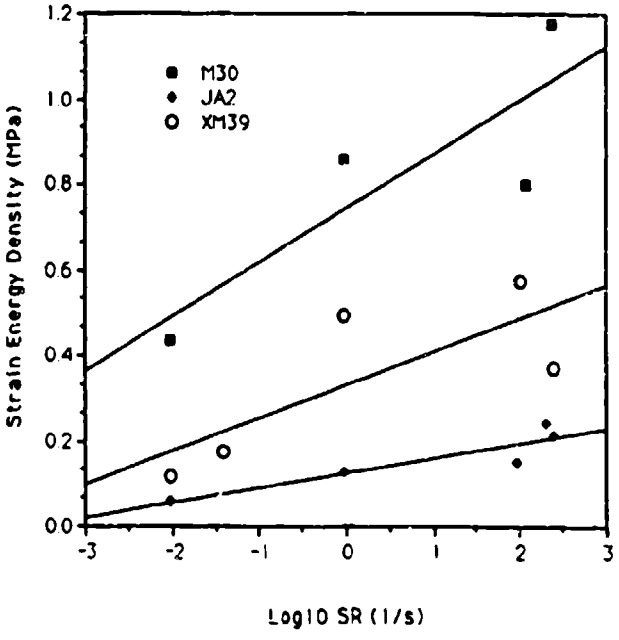

Figure 7. Strain Energy versus Strain Rate.

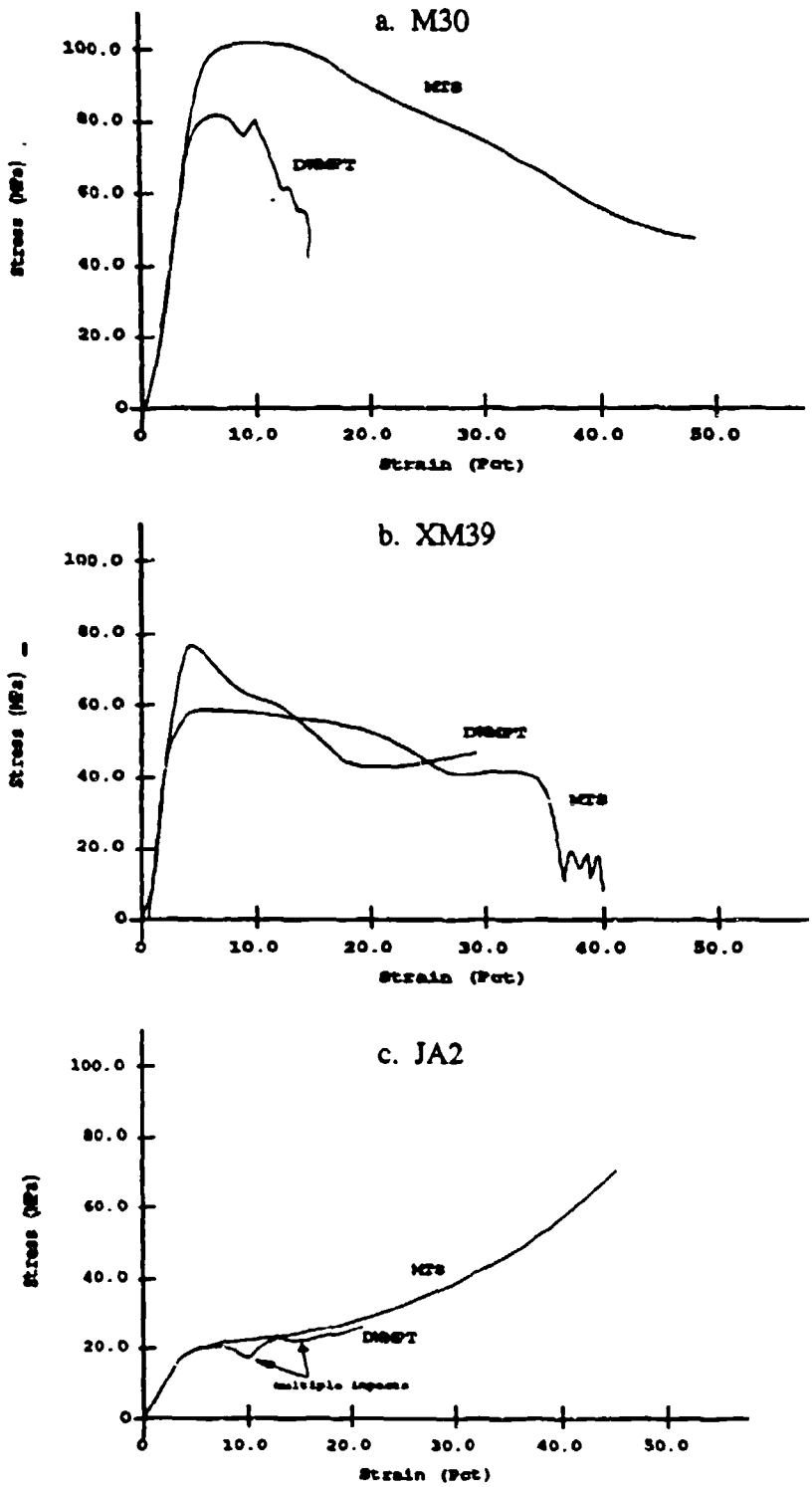

Figure 8. Representative Stress versus Strain Curves which Compare the Mechanical Response of M30, XM39, and JA2 Propellants at Room Temperature and a Strain Rate of 250 sec^{-1}.

5. ABSORBED STRAIN ENERGY DENSITY

5.1 Cumulative Absorbed Strain Energy Density. The cumulative strain energy density per unit volume, τ, absorbed by M30, XM39, and JA2 propellants at increasing increments of strain (to 30 percent) versus strain rate are illustrated in contour maps and 3-dimensional surfaces (Appendix B). The cumulative strain energy density was greater for the work-softening M30 and XM39 propellants with maxima at 23 and 16 MPa respectively. This is because much higher stress levels were attained during the deformation of these materials. The maximum strain energy density for the work-hardening JA2 propellant is only 7 MPa at 30 percent strain. All three propellants are macroscopically ductile yet M30 and XM39 propellants fractured and work-softened and JA2 flowed and work-hardened during deformation. However, the macroscopic ductility in JA2 could be accommodated by a microphysical fracture deformation mechanism and future experiments carried to fixed amounts of total strain are planned in an effort to study the phenomenon.

5.2 Incremental Absorbed Strain Energy Density. The normalized incremental strain energy density, Γ, absorbed by M30, XM39, and JA2 propellants determined at increments between 0 and 10, 10 and 20, and 20 and 30 percent strain versus strain rate are illustrated in contour maps and 3-dimensional surfaces (Appendix C). The contours in these plots are normalized to the maximum cumulative strain energy absorbed as described in the previous section. The dimensionless Γ contour maps reveal that the M30 and XM39 propellants possess a saddle with maximum Γ of about .4, and strain increment between 10 and 20 percent. This behavior is expected since the stress strain curves for M30 and XM39 work-soften after the maximum stress has been reached. The Γ contour map for JA2, however, does not possess a saddle but continually increases; this behavior is also expected for macroscopically ductile work-hardening materials.

6. TIME DEPENDENT MECHANICAL PROPERTIES

The following section includes some initial results on the viscoelastic characterization of M30, XM39, and JA2 propellants. Since perforated specimens were tested, the measured response contains both structural and material contributions. It may be impossible to determine the intrinsic material properties for these materials since extruded propellants with multiple perforations possess a directional anisotropy not present in the solid material. Furthermore, the determination of constitutive equations for materials requires that the boundary value problem be homogeneous, viz., the stresses within the continuum be identical to those applied at the boundary. Real world testing conditions only approach this requirement, and in the final analysis the results of testing perforated specimens will be no better than for any material that contains large internal voids or pores.

6.1 Linear Viscoelasticity Theory. A material exhibits linear behavior in response to a generalized input if the following two conditions are satisfied:

1) $R[I_a + I_b] = R[I_a] + R[I_b]$ Superposition Property

2) $R[cI] = cR[I]$ Homogeneity Property

where I, I_a, and I_b are general input histories and the brackets [ ], are used to denote that the current value of R depends on the history of I and not just its instantaneous value. Following the notation of Schapery[14,17], if a material is linear, the response R(t) to a general input I(t) can be written as:

$$R(t) = \int_{-\infty}^{t} R_H(t-\tau) \frac{dI}{d\tau} d\tau$$

The above relation connecting input and response is commonly referred to by various names such as, hereditary integral, superposition integral, Duhamel's integral, or convolution integral. $R_H(t)$ is the unit response function for a nonaging material (viz. a material whose material properties do not depend on the time they are tested). In a creep test, $R_H(t) = D(t) = \varepsilon(t)/\sigma_o$ where D(t) is the creep compliance and is experimentally determined by performing a creep test while applying a constant stress input, $I = \sigma_o H(t)$ (Figure 9). H(t) is the Heaviside step function defined as: H(arg) = 1, arg > 0; H(arg) = 0, arg < 0. In a relaxation test, $R_H(t) = E(t) = \sigma(t)/\varepsilon_o$ where E(t) is the relaxation modulus and is experimentally determined by performing a relaxation test while applying a constant strain input, $I = \varepsilon_o H(t)$ (Figure 10).

Some common linear creep compliances that are often used in the literature include the power law $D(t) = Do + D_1 t^m$, and Maxwell $D(t) = Do + t/\eta$ viscoelastic rheologies. Writing the convolution integral in terms of one-dimension yields for strain and stress:

$$\varepsilon(t) = \int_{-\infty}^{t} D(t-\tau) \frac{dI}{d\tau} d\tau \qquad (5)$$

$$\sigma(t) = \int_{-\infty}^{t} E(t-\tau) \frac{dI}{d\tau} d\tau \qquad (6)$$

where D(t) is the creep compliance and E(t) is the relaxation modulus. Once the relaxation modulus is experimentally determined, the stress as a function of time is expressed for an arbitrary strain input with Equation 6. Equations 5 and 6 form the one-dimensional constitutive equations for a linear viscoelastic nonaging material.

6.2 Constant Strain Rate Test. The input for a constant strain rate test is given by:

$$\varepsilon(t) = c\, t\, H(t) \qquad (7)$$

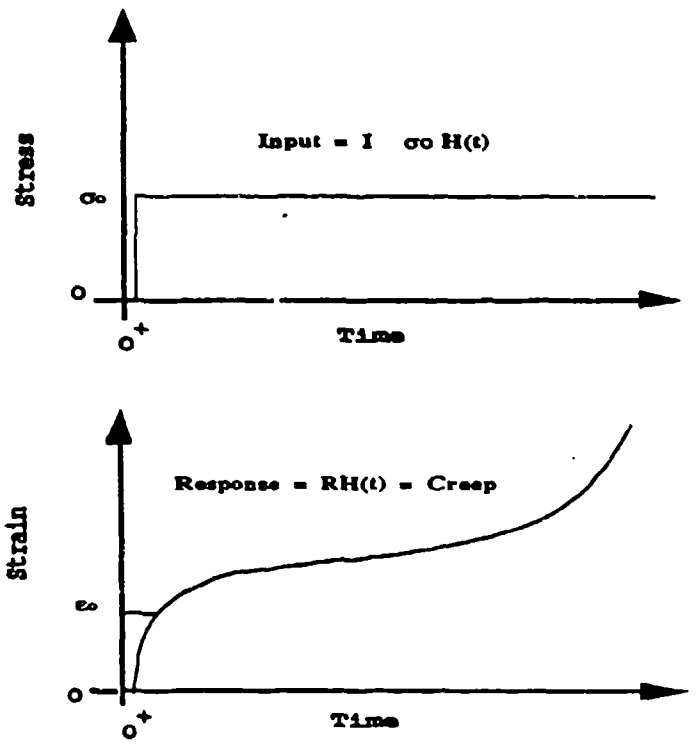

Figure 9. Creep Response to a Unit Input in Stress.

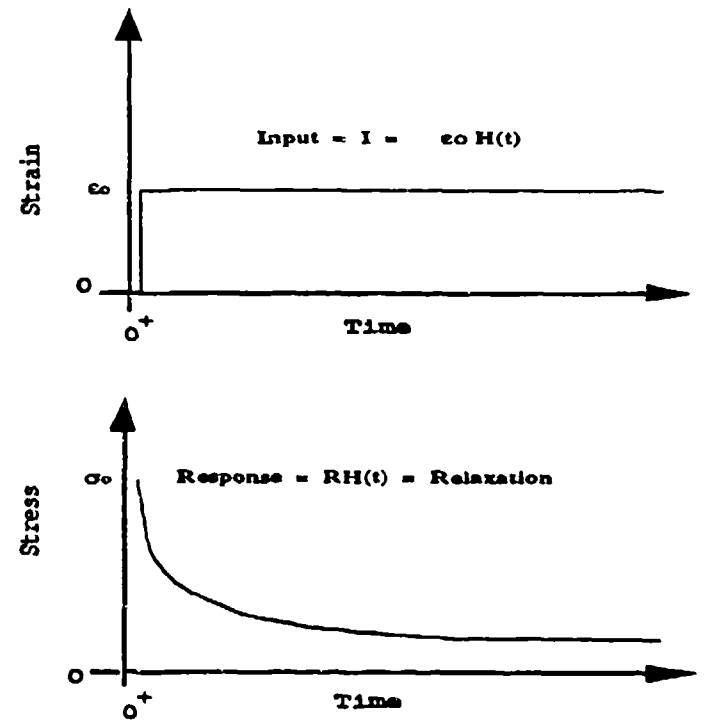

Figure 10. Relaxation Response to a Unit Input in Strain.

where c is the constant strain rate. Substitution of Equation 7 into Equation 6 with a change of variables u=t-τ, and assuming that $E(t-\tau) = 0$ for $t < \tau$ gives:

$$\sigma(t) = c \int_0^t E(u)\, du \qquad t > 0 \tag{8}$$

differentiating both sides of the Equation 8 with respect to time gives the relaxation modulus:

$$E(t) = d\sigma/d\varepsilon \tag{9}$$

This shows that the relaxation modulus is obtainable from a constant strain rate experiment and is equal to the tangent modulus, which is the local tangent to the stress versus strain curve taken at times, $t = \varepsilon/c$. It can also be shown that the relaxation modulus is related to the secant modulus, defined as:

$$E_s = \sigma/\varepsilon \tag{10}$$

The secant modulus can be written by substituting Equation 8 into Equation 10, which gives:

$$E_s = 1/t \int_0^t E(u)\, du \qquad t > 0 \tag{11}$$

Differentiating both sides of Equation 11 and solving for E(t) gives:

$$E(t) = E_s + t\, dE_s/dt \tag{12}$$

Equation 12 can be written as:

$$E(t) = E_s[1. + (dE_s/E_s)/(dt/t)] \tag{13}$$

Using a property of logarithms[14,15] (i.e. $\ln 10\, d(\log_{10} x) = dx/x$), Equation 13 can be rewritten as:

$$E(t) = E_s\,[1. + d(\log_{10} E_s)/d(\log_{10} t)] \tag{14}$$

Note that if the slope of the $\log E_s$ versus $\log t$ curve is much less than one, then the relaxation modulus, E(t), is nearly identical to the secant modulus, E_s. Furthermore, since both E(t) and E_s are both functions only of time, if any strain level dependence is observed the material is nonlinear.

To determine the relaxation moduli, secant moduli and to test for linear/nonlinear viscoelastic behavior for the M30, XM39, and JA2 propellants, we use the constant strain rate data and plot the log of the secant modulus (Equation 10) versus log time (Appendix D). The time is determined by $t = \varepsilon/c$, where ε is the fixed strain level and c is the strain rate. As an example, the relaxation and secant moduli are determined from the JA2 test data taken at different strain rates (Figure 11) and plotted as a function of time at strain levels of 5, 10, 20 and 30 percent in Figure D1. The lines in Figure D1 represent the moduli determined at different strain levels as defined by the symbols in Figure 11. By using data taken from several tests over a wide range of strain rates, the relaxation

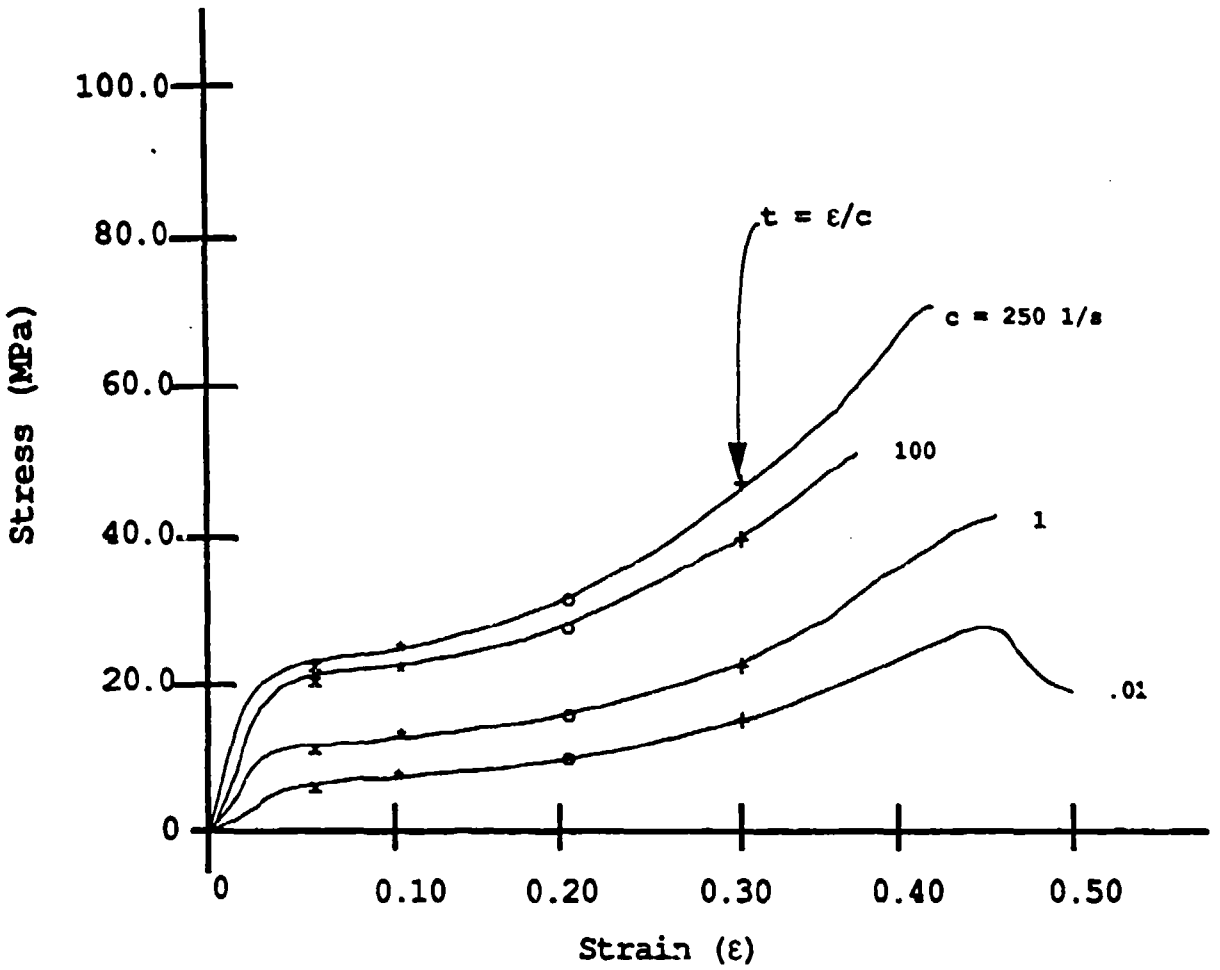

Figure 11. Graphical Means for Determining Relaxation Moduli (Appendix D) for JA2 Tested at Various Strain Rates.

and secant moduli can be determined for the material for times which range over many orders of magnitude. All three propellants exhibit a strong nonlinear response as evidenced by the strain level dependence of the secant modulus. The slopes of the $\log E_t$ versus $\log t$ curves are much less than one, so the relaxation modulus (dashed lines in Appendix D) can be well represented by the secant modulus. Data from the Split Hopkinson Bar are also included and indicate good experimental agreement with secant moduli determined over a wide range of strain rates from 10^{-2} to 10^{+4}. The room-temperature relaxation modulus for these propellants can be represented by a power-law of the form:

$$E(t) = E_1 t^n \tag{15}$$

Laplace transforms can be used to show that a good approximation of the creep compliance is:

$$D(t) = E(t)^{-1} \tag{16}$$

which is in error by at most 10 % when $0 < n < .25$ in Equation 15[14]. For linear materials, the relaxation and creep compliances are directly substituted into Equations 5 and 6, and the one-dimensional stress and strain response for the propellant can be determined for any arbitrary stress or strain input history. This procedure cannot be applied for nonlinear functionals however, but can be treated using the multiple integral representations of nonlinear viscoelasticity[16] or an alternative formulation[17] whereby the relaxation moduli are vertically shifted to form "master" curves. This procedure is similar to the horizontal time-temperature shifting procedure performed on thermorheologically simple materials[14].

7. SUMMARY AND CONCLUSIONS

This report describes the preliminary results of a series of mechanical property tests for the room temperature, uniaxial compression of M30, XM39, and JA2 gun propellants at strain rates of .01, 1, 100, and 250 per second using the Ballistic Research Laboratory's new High Rate servohydraulic test apparatus.

Using a linear elastic model, the apparatus stiffness is determined to be about 92 kN/mm. The strain energy absorbed at yield for a "typical" propellant grain is 7 times greater than the energy stored in the apparatus, so that the complete post-failure stress versus strain curve can be traced using the servohydraulic test apparatus. The compressive moduli determined with the servohydraulic apparatus compare favorably with those determined using the Drop Weight test apparatus at a strain rate of 250 per second. However, the post-failure behaviors of M30 and XM39 tested on these apparatuses do not compare well, and are probably a consequence of differing input strain histories imparted to the specimens on each of the apparatuses in the post-failure regime. This hypothesis might be verified by simulating a strain history input from a typical Drop Weight test on the servohydraulic apparatus, and observing whether the post-failure responses are comparable.

The compressive modulus, yield stress, and absorbed strain energy at yield all increase for these propellants as a function of strain rate, whereas the yield strain remains relatively constant and independent of strain rate. The M30 and XM39 propellants macroscopically failed by fracture at all strain rates tested. The JA2 propellant did not fracture but macroscopically flowed during the entire

deformation history. Microfracturing could be a mechanism for macroscopic flow and ductility so that detailed microstructural observations are necessary to determine when and if fracturing begins, since it is at this time that additional surface area becomes available for burning.

A preliminary viscoelastic characterization indicates that all three propellants exhibit nonlinear behavior. Since the specimens contain perforations, both a structural and material contribution to the nonlinearity is present. In order to obtain stress homogeneity within specimens, testing for constitutive properties is normally performed on solid specimens. This may not be valid for propellants since the extrusion process imparts a directional anisotropy oriented along the grain axis not present in solid grains. For the present then, we will consider these tests as "pseudo" constitutive tests, the results of which are no better than any material which contains voids, large pores or other internal inhomogeneities.

The room temperature secant and relaxation moduli for these propellants can be represented by a power law in time for strain rates which range from 10^{-2} to 10^{-4} sec^{-1}. The relaxation moduli determined from tests at strain rates greater than 250 sec^{-1} are obtained from Split Hopkinson Bar tests[5] and are linearly extrapolatable from the servohydraulic test results conducted at lower strain rates.

8. FUTURE WORK

8.1 Microstructural Observations. Future work should focus on detailed scanning electron microscope and optical microscope observations of the deformation mechanisms to determine when microfracturing begins to occur in these propellants. A vacuum impregnation epoxy technique might be used to help maintain grain integrity, since these propellants are relatively soft and can be damaged during preparation for optical examination. The technique has been used for examining deformation mechanisms in crystalline materials and involves vacuum impregnating deformed specimens with dyed epoxy, hardening, and finally thin-sectioning and polishing the specimens. Tests where specimens are deformed to fixed amounts of total strain will permit the characterization of microstructural changes within the propellant, and determine when and under what conditions fractures begin to form. Mini closed-bomb tests should also be an integral part of the testing program, so that we can correlate the combustion characteristics of propellants, deformed to fixed amounts of total strain, to the macroscopic mechanical property parameters determined from the stress versus strain curves.

8.2 Interior Ballistics Modeling. Interior ballistics modeling will require data which characterize both the constitutive properties and a generalized failure criterion for propellants. A nonlinear viscoelastic constitutive characterization of the propellant which includes a damage model is presently being developed; a generalized failure criterion based on stress or strain invariants will require tests performed in compression, tension and torsion. The development of a generalized failure criterion is necessary since propellant grains are subjected to combined stress states within the gun cartridge during the ballistic cycle.

INTENTIONALLY LEFT BLANK.

9. REFERENCES

1. R.J. Lieb, "Impact-Generated Surface Area in Gun Propellants," Technical Report BRL-TR-2946, AD A200468, USA Ballistic Research Laboratory, Aberdeen Proving Ground, Maryland, November 1988.

2. J.C. Jaeger, N.G. Cook, "Fundamentals of Rock Mechanics," 3rd Edition, Chapman & Hall, London, 1979.

3. R.J. Lieb, and J.J. Rocchio, "A Gas Gun Impact Tester for Solid Gun Propellants," Memo randum Report BRL-MR-3399, USA Ballistic Research Laboratory, Aberdeen Proving Ground, Maryland, October 1984.

4. R.J. Lieb, and J.J. Rocchio, "Standardization of a Drop Weight Mechanical Properties Tester for Gun Propellants," Technical Report ARBL-TR-02516, USA ARRADCOM Bal listic Research Laboratory, Aberdeen Proving Ground, Maryland, July 1983.

5. R.J. Lieb, T.J. Fischer, and H.J. Hoffman, "High Strain Rate Response of Gun Propellant Using the Hopkinson Split Bar," JANNAF Structures and Mechanics Behavior Proceedings, November, 1989.

6. J.A. Birkett, "The Acquisition of M30A1 Propellant Rheology Data," Indian Head Technical Report 724, Indian Head, Maryland, September 1981.

7. R.J. Lieb, "High Rate Intrinsic Bed Response of Gun Propellant," JANNAF Structures and Mechanical Behavior Subcommittee Meeting, CPIA Publication 463, 51-62, March, 1987.

8. R.L. Campbell, W.L. Elban, and P.J. Coynes Jr., "Side-Wall Pressure Measurements in Quasi-static Compaction of Porous Beds of HMX Powders and ABL 2523 Casting Pow der," Proceedings in 1988 Propulsion Systems Hazards Subcommittee Meeting, CPIA Publication 477, 1-15, March, 1988.

9. W.G. Soper, "Ignition Waves in Gun Chambers," Combustion and Flame, v. 20, 157-162, 1973.

10. W.G. Soper, "Grain Velocities During Ignition of Gun Propellant," Combustion and Flame, v. 24, 199-202, 1975.

11. L.M. Chang, "Ignition Diagnostics of the 120-mm XM859- MP Cartridge," Technical Report BRL-TR-2840, USA Ballistic Research Laboratory, Aberdeen Proving Ground, Maryland, August 1987.

12. C.F. Fong, and B.K. Moy, "Ballistic Criteria for Propellant Grain Fracture in the GAU-8/A 30-mm Gun," AFATL-TR-82-21, Eglin Air Force Base, Florida, March 1982.

13. R.J. Lieb, "The Mechanical Response of M30, JA2, and XM39 Gun Propellant to High Rate Deformation," Technical Report (BRL-TR-3023) USA BRL, Aberdeen Proving Ground, August, 1989.

14. R.A. Schapery "Viscoelastic Behavior and Analysis of Composite Materials," Mechanics of Composite Materials, v. 2, Edited by G.P. Sendeckyj, Academic Press, 85-168, 1974.

15. T.L. Smith, "Evaluation of the Relaxation Modulus From the Response to a Constant Rate of Strain Followed by a Constant Strain," Journal of Polymer Science, v. 17, 2181-2188, 1979.

16. W.N. Findley, and J.S. Lai, "A Modified Superposition Principle Applied to Creep of Non inear Viscoelastic Material Under Abrupt Changes in Combined Stress," Trans. Soc. Rheol., v. 11, no. 3, 361-380, 1967.

17. G.A. Gazonas, MM 651, " Viscoelasticity I" class notes taught by R.A. Schapery, Texas A&M University, Fall 1980.

APPENDIX A:
REPRESENTATIVE STRESS VERSUS STRAIN RESPONSE FOR JA2, M30, AND XM39

INTENTIONALLY LEFT BLANK.

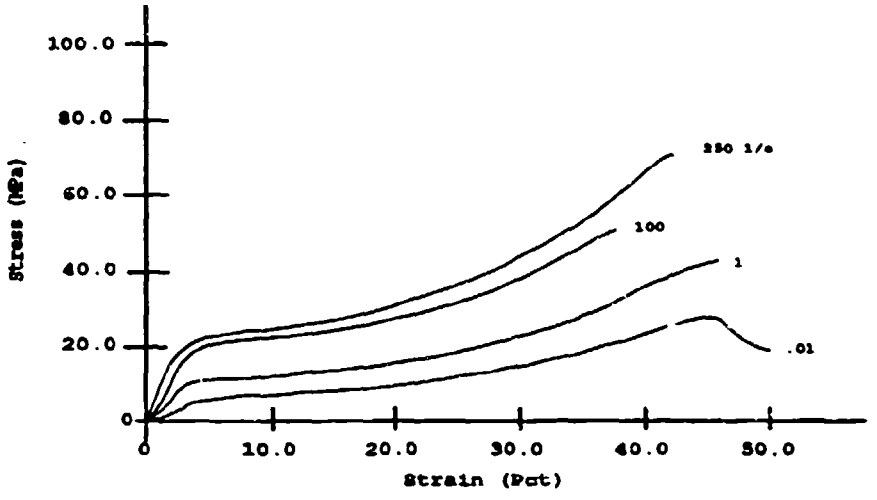

Figure A1. Representative Stress versus Strain Response for JA2

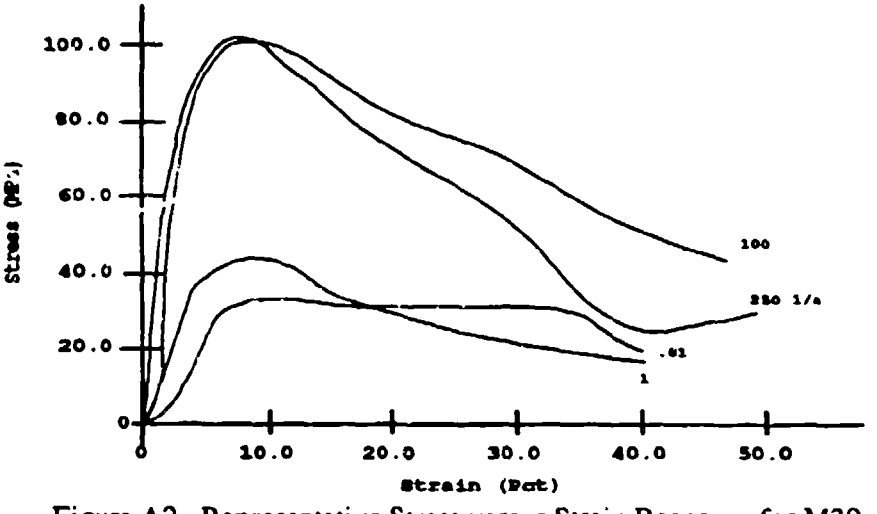

Figure A2. Representative Stress versus Strain Response for M30

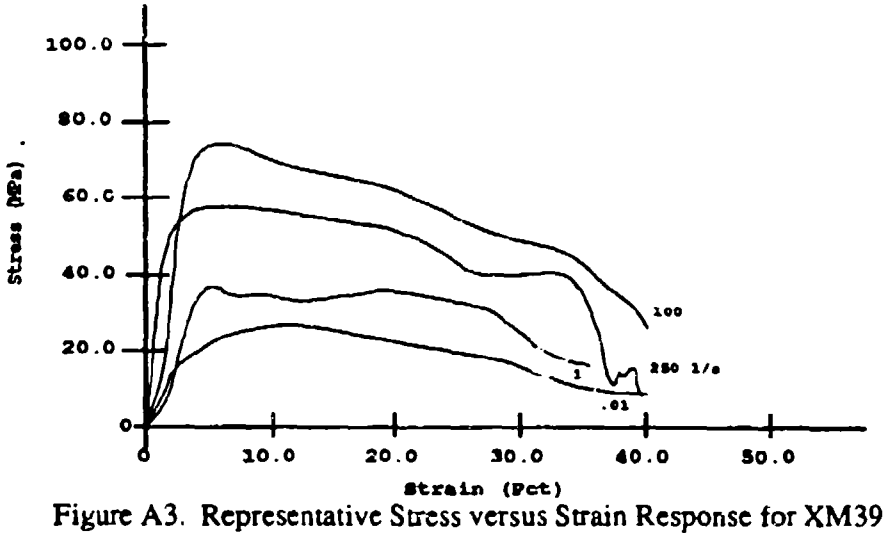

Figure A3. Representative Stress versus Strain Response for XM39

INTENTIONALLY LEFT BLANK.

APPENDIX B:
CUMULATIVE ABSORBED STRAIN ENERGY DENSITY MAPS

INTENTIONALLY LEFT BLANK.

Figure B1. Cumulative Absorbed Strain Energy Density Map for **JA2**

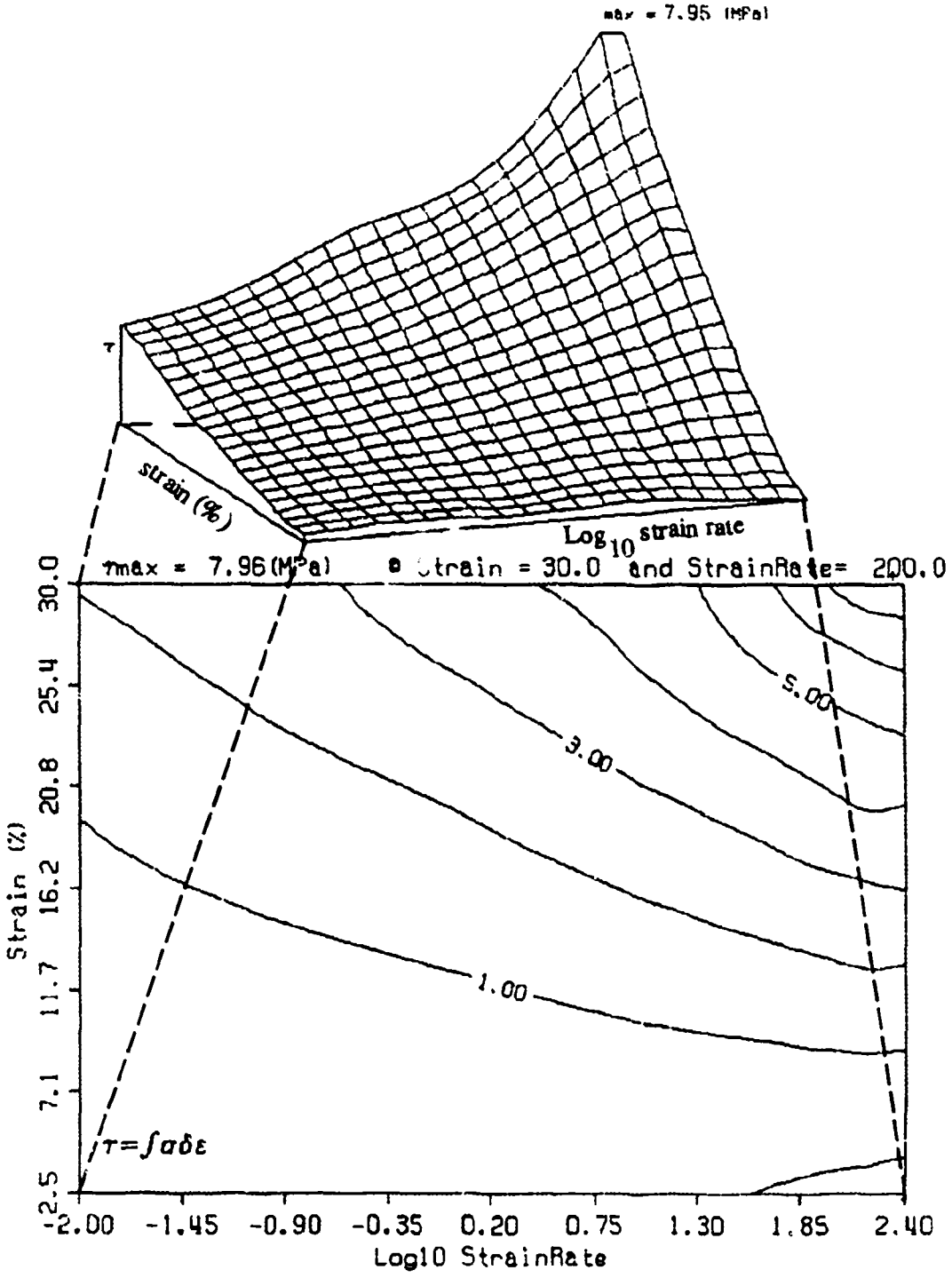

Figure B2. Cumulative Absorbed Strain Energy Density Map for **M30**

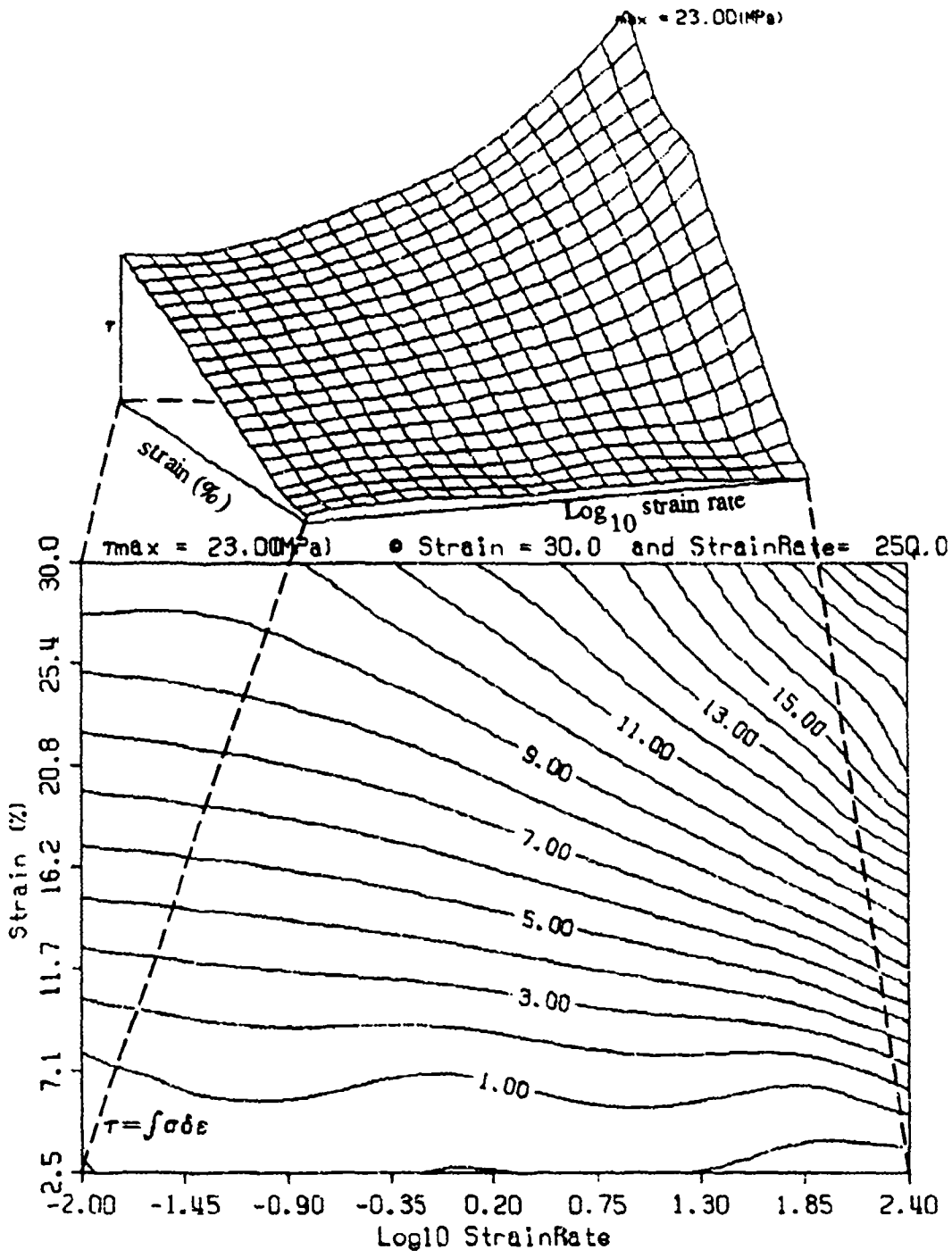

Figure B3. Cumulative Absorbed Strain Energy Density Map for **XM39**

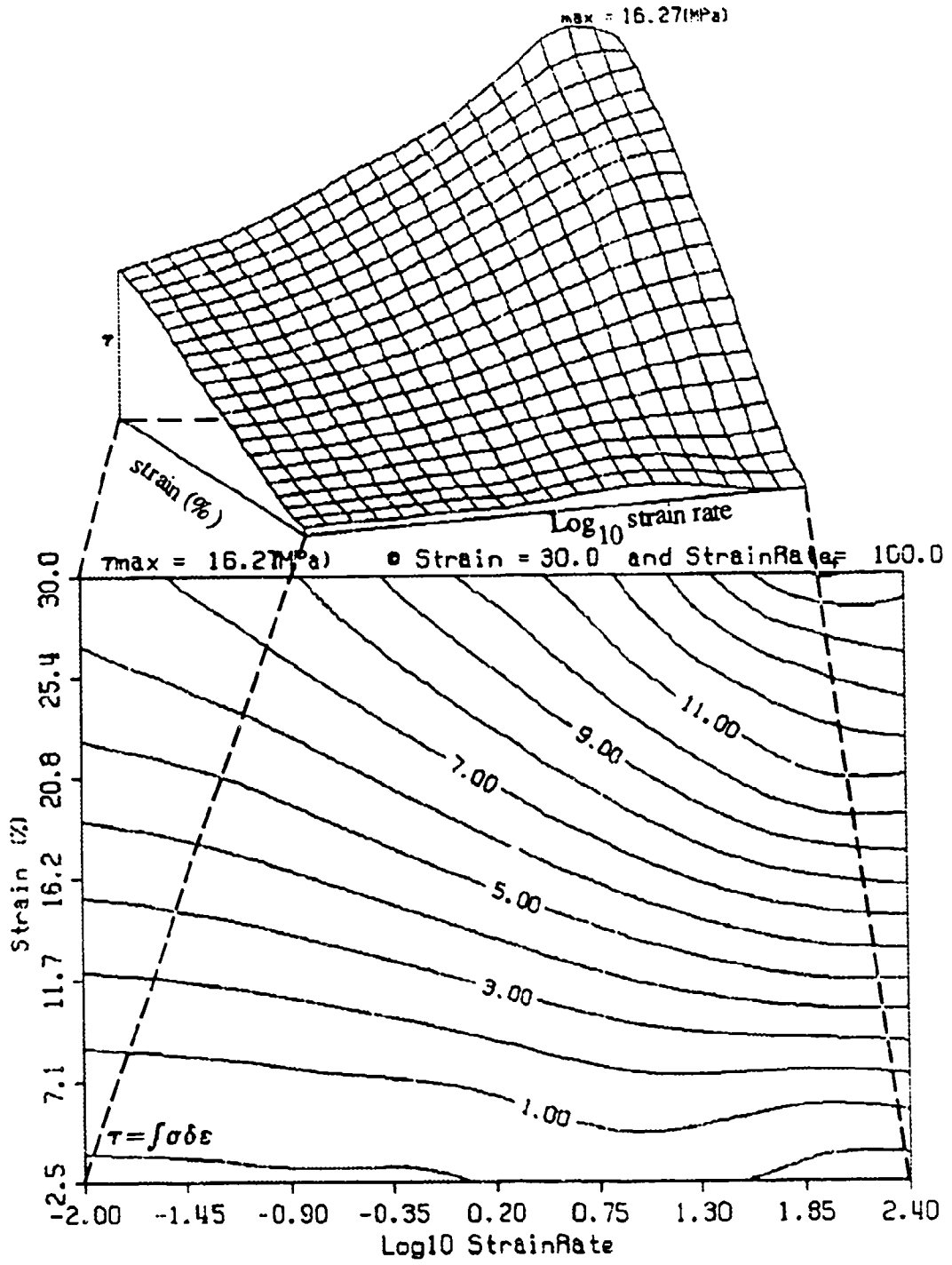

INTENTIONALLY LEFT BLANK.

APPENDIX C:
INCREMENTAL ABSORBED STRAIN ENERGY DENSITY MAPS

INTENTIONALLY LEFT BLANK.

Figure C1. Incremental Absorbed Strain Energy Density Map for **JA2**

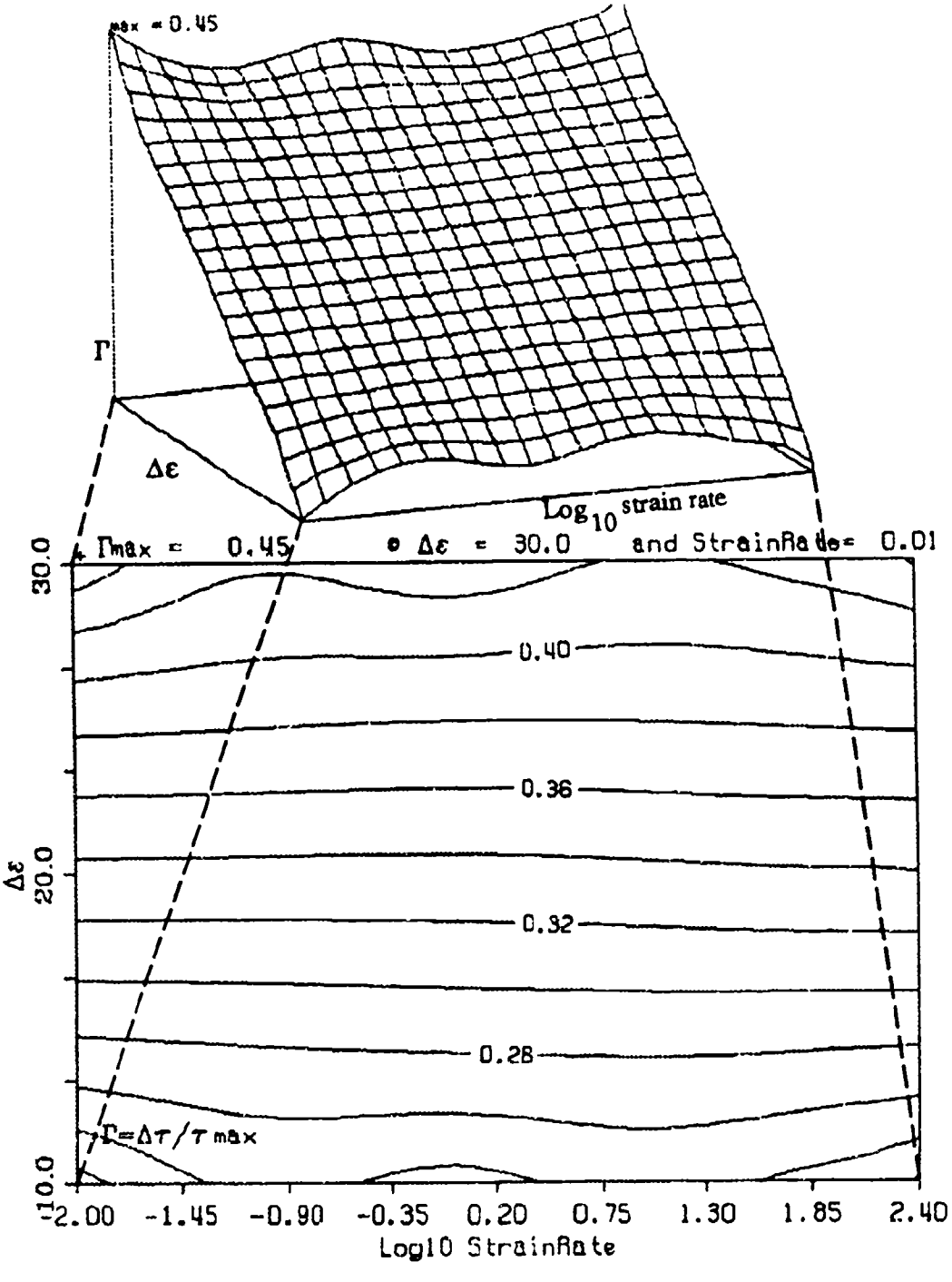

Figure C2. Incremental Absorbed Strain Energy Density Map for **M30**

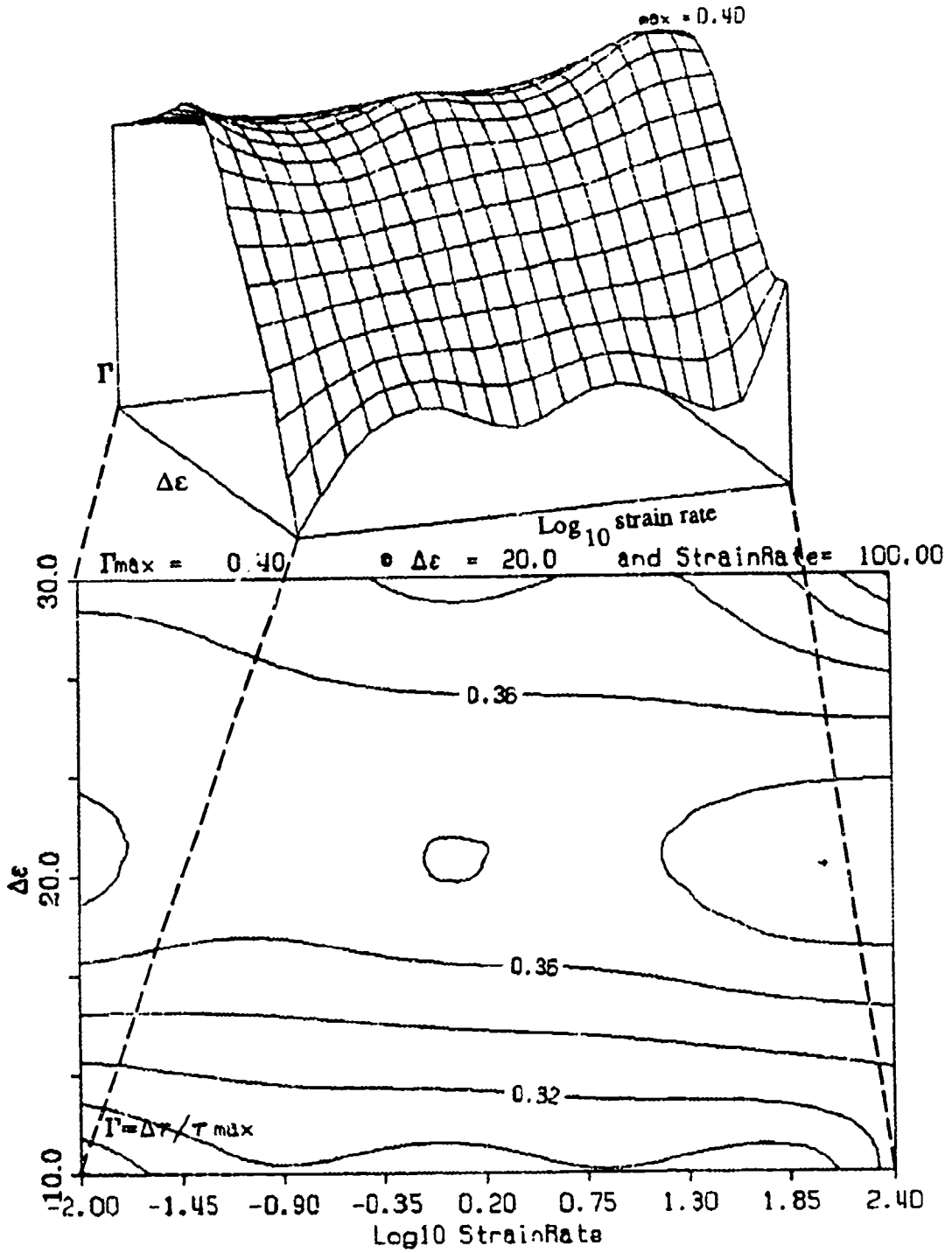

Figure C3. Incremental Absorbed Strain Energy Density Map for **XM39**

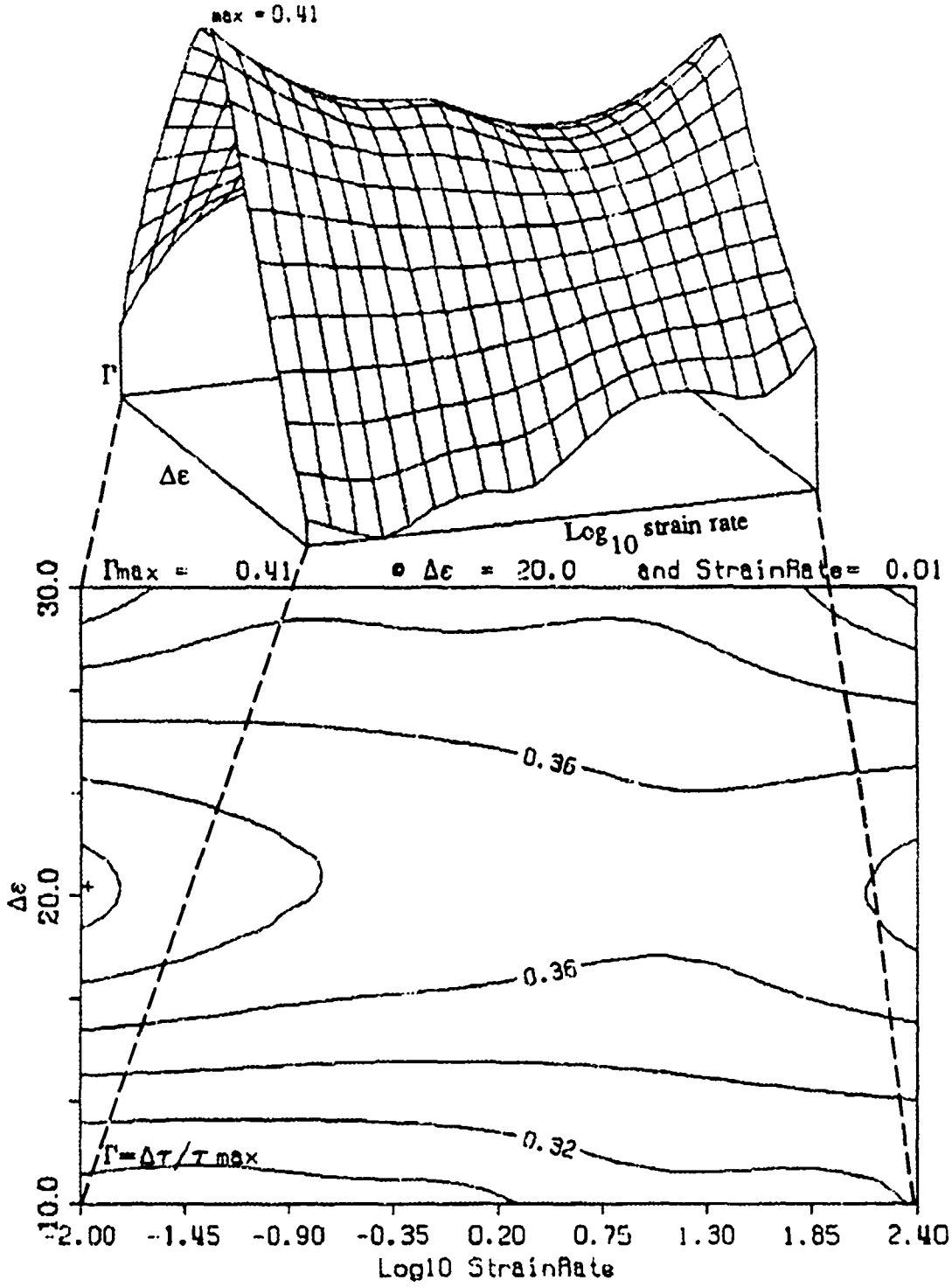

INTENTIONALLY LEFT BLANK.

APPENDIX D:
RELAXATION MODULI FOR JA2, M30, AND XM39 PROPELLANTS

INTENTIONALLY LEFT BLANK.

Figure D1. JA2 Relaxation Moduli

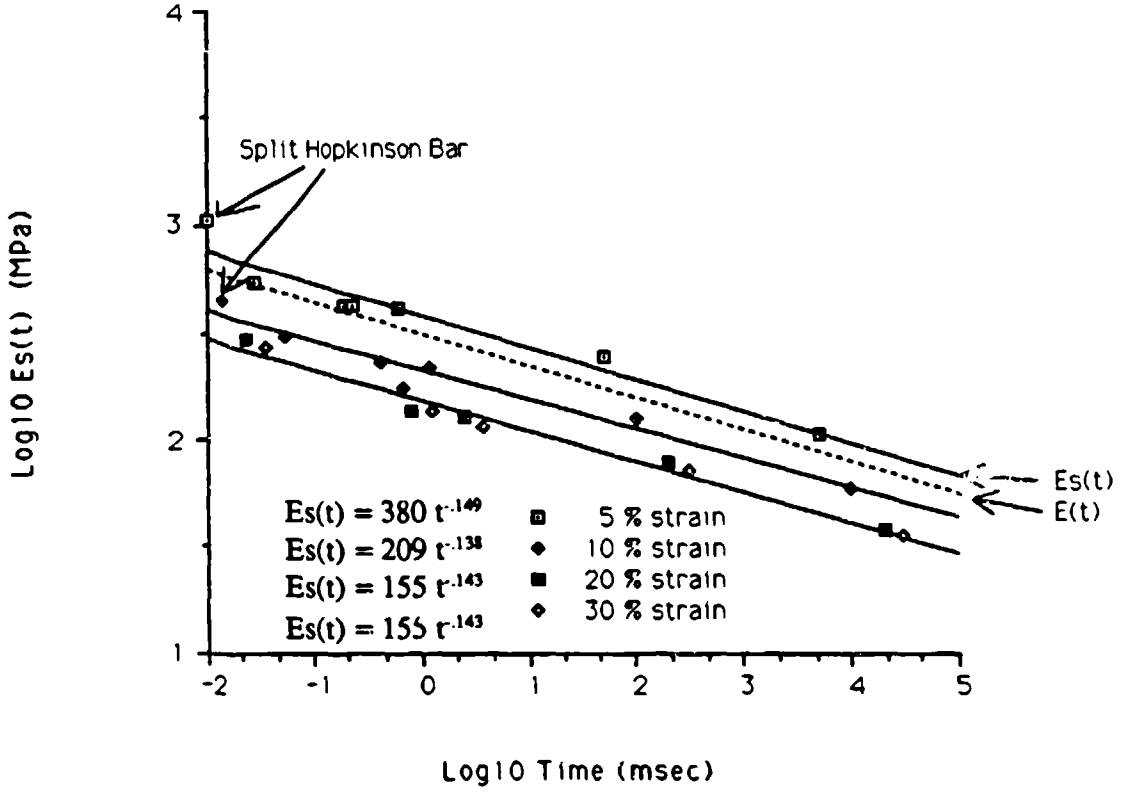

Figure D2. M30 Relaxation Moduli

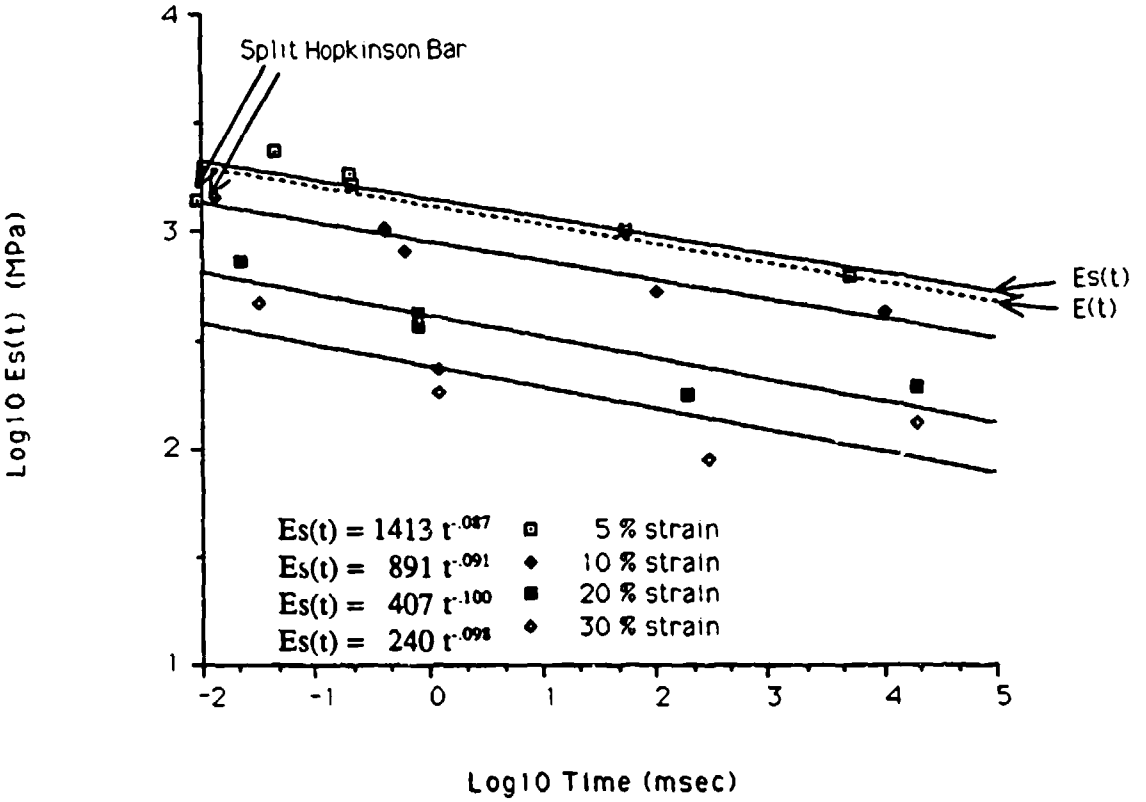

Figure D3. XM39 Relaxation Moduli

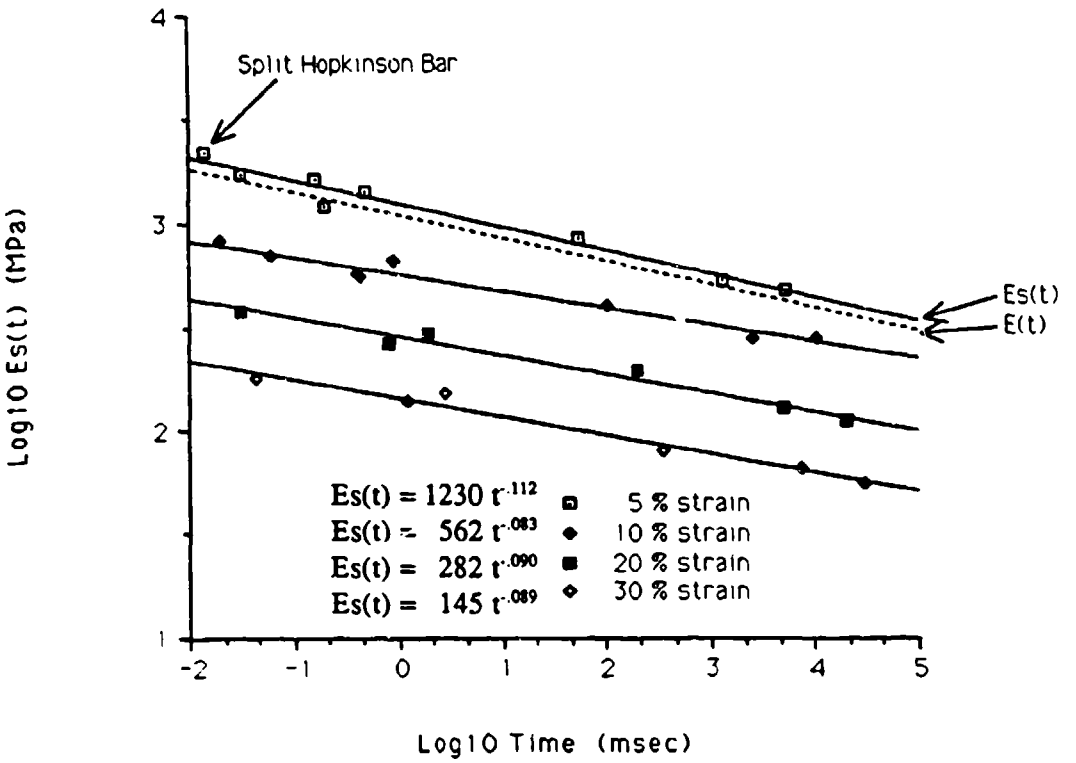

INTENTIONALLY LEFT BLANK.

No of Copies	Organization
2	Administrator Defense Technical Info Center ATTN: DTIC-DDA Cameron Station Alexandria, VA 22304-6145
1	HQDA (SARD-TR) WASH DC 20310-0001
1	Commander US Army Materiel Command ATTN: AMCDRA-ST 5001 Eisenhower Avenue Alexandria, VA 22333-0001
1	Commander US Army Laboratory Command ATTN: AMSLC-DL Adelphi, MD 20783-1145
2	Commander US Army, ARDEC ATTN: SMCAR-IMI-I Picatinny Arsenal, NJ 07806-5000
2	Commander US Army, ARDEC ATTN: SMCAR-TDC Picatinny Arsenal, NJ 07806-5000
1	Director Benet Weapons Laboratory US Army, ARDEC ATTN: SMCAR-CCB-TL Watervliet, NY 12189-4050
1	Commander US Army Armament, Munitions and Chemical Command ATTN: SMCAR-ESP-L Rock Island, IL 61299-5000
1	Director US Army Aviation Research and Technology Activity ATTN: SAVRT-R (Library) M/S 219-3 Ames Research Center Moffett Field, CA 94035-1000

No of Copies	Organization
1	Commander US Army Missile Command ATTN: AMSMI-RD-CS-R (DOC) Redstone Arsenal, AL 35898-5010
1	Commander US Army Tank-Automotive Command ATTN: AMSTA-TSL (Technical Library) Warren, MI 48397-5000
1	Director US Army TRADOC Analysis Command ATTN: ATRC-WSR White Sands Missile Range, NM 88002-5502
(Class. only) 1	Commandant US Army Infantry School ATTN: ATSH-CD (Security Mgr.) Fort Benning, GA 31905-5660
(Unclass. only) 1	Commandant US Army Infantry School ATTN: ATSH-CD-CSO-OR Fort Benning, GA 31905-5660
1	Air Force Armament Laboratory ATTN: AFATL/DLODL Eglin AFB, FL 32542-5000
	Aberdeen Proving Ground
2	Dir, USAMSAA ATTN: AMXSY-D AMXSY-MP, H. Cohen
1	Cdr, USATECOM ATTN: AMSTE-TD
3	Cdr, CRDEC, AMCCOM ATTN: SMCCR-RSP-A SMCCR-MU SMCCR-MSI
1	Dir, VLAMO ATTN: AMSLC-VL-D

No. of
Copies Organization

1 HQDA (SARDA)
WASH, DC 20310-2500

1 Commander
USA Concepts Analysis Agency
ATTN: D. Hardison
8120 Woodmont Ave.
Bethesda, MD 20014-2797

1 Commander
US Army Materiel Command
ATTN: AMCDE-DW
5001 Eisenhower Ave.
Alexandria, VA 22333-5001

1 PEO-Armaments
Project Manager
Autonomous Precision-Guided
Munition (APGM)
US Army, ARDEC
ATTN: AMCPM-CWW
Picatinny Arsenal, NJ 07806-5000

1 PEO-Armaments
Project Manager
Autonomous Precision-Guided
Munition (APGM)
US Army, ARDEC
ATTN: AMCPM-CWA-S, R. DeKleine
Picatinny Arsenal, NJ 07806-5000

1 Commander
Production Base
Modernization Agency
US Army, ARDEC
ATTN: AMSMC-PBM-E, L. Laibson
Picatinny Arsenal, NJ 07806-5000

1 PEO-Armaments
Project Manager
Tank Main Armament Systems
US Army, ARDEC
ATTN: AMCPM-TMA-105
Picatinny Arsenal, NJ 07806-5000

No. of
Copies Organization

1 US Army Ballistic Missile
Defense Systems Command
Advanced Technology Center
PO Box 1500
Huntsville, AL 35807-3801

1 Project Manger
Autonomous Precision-Guided
Munition (APGM)
US Army, ARDEC
ATTN: AMCOM-CWW, F. Menke
Picatinny Arsenal, NJ 07806-5000

1 PEO-Armaments
Project Manager
Autonomous Precision-Guided
Munition (APGM)
US Army, ARDEC
ATTN: AMCPM-CWS, M. Fisette
Picatinny Asenal, NJ 07806-5000

1 PEO-Armaments
Project Manager
Autonomous Precision-Guided
Munition (APGM)
US Army, ARDEC
ATTN: AMCPM-CWA, H. Hassmann
Picatinny Arsenal, NJ 07806-5000

1 PEO-Armaments
Project Manager
Tank Main Armament Systems
ATTN: AMCPM-TMA, K. Russell
Picatinny Arsenal, NJ 07806-5000

1 PEO-Arments
Project Manager
Tank Main Armament Systems
ATTN: AMCPM-TMA-120
Picatinny Arsenal, NJ 07806-5000

1 Chairman
DOD Explosives Safety Board
Room 856-C, Hoffman Bldg. 1
2461 Eisenhower Ave.
Alexandria, VA 22331-0600

No. of
Copies Organization

1 Commander
US Army Materiel Command
ATTN: AMCPM-GCM-WF
5001 Eisenhower Ave.
Alexandria, VA 22333-5001

1 Commander
US Army, ARDEC
ATTN: SMCAR-AEE-B, D. Downs
Picatinny Arsenal, NJ 07806-5000

1 Commander
US Army, ARDEC
ATTN: SMCAR-AES
Picatinny Arsenal, NJ 07806-5000

1 Commander
US Army, ARDEC
ATTN: SMCAR-HFM, E. Barrieres
Picatinny Arsenal, NJ 07806-5000

1 Commander
US Army, ARDEC
ATTN: SMCAR-CCH-V, C. Mandala
Picatinny Arsenal, NJ 07806-5000

1 Commander
US Army, ARDEC
ATTN: SMCAR-AEE-B, B. Brodman
Picatinny Arsenal, NJ 07806-5000

1 Commander
US Army Harry Diamond Laboratories
ATTN: SLCHD-TA-L
2800 Powder Mill Road
Adelphi, MD 20783-1145

1 Commandant
US Army Aviation School
ATTN: Aviation Agency
Fort Rucker, AL 36360

1 Commander, USACECOM
R&D Technical Library
ATTN: ASQNC-ELC-I-T, Myer Center
Fort Monmouth, NJ 07703-5301

No. of
Copies Organization

1 Project Manager
US Army Tank-Automotive
Command
ATTN: AMCPM-ABMS
Warren, MI 48092-2498

1 Commander
US Army, ARDEC
ATTN: SMCAR-HFM, R. Davitt
Picatinny Arsenal, NJ 07806-5000

1 Commander
US Army, ARDEC
ATTN: SMCAR-FSA-T, M. Salsbury
Picatinny Arsenal, NJ 07806-5000

1 Commander
US Army TSARCOM
4300 Goodfellow Blvd.
St. Louis, MO 63120-1702

1 Commander
US Army Missile and Space
Intelligence Center
ATTN: AIAMS-YDL
Redstone Arsenal, AL 35898-5500

1 Commander
US Army Tank-Automotive
Command
ATTN: AMSTA-CG
Warren, MI 48090

1 President
US Army Armor & Engineer
Board
ATTN: ATZK-AD-S
Fort Knox, KY 40121-5200

1 Director
HQ, TRAC RPD
ATTN: ATRC-MA (MAJ Williams)
Fort Monroe, VA 23651

2 Commander
US Army Materials Technology
Laboratory
ATTN: SLCMT-ATL
Watertown, MA 02172-0001

No. of Copies	Organization
2	Program Manager US Army Tank-Automotive Command ATTN: AMCPM-ABMS, T. Dean Warren, MI 48092-2498
1	Office of Naval Research ATTN: Code 473, R. S. Miller 800 N. Quincy St. Arlington, VA 22217-9999
1	Commandant US Army Special Warfare School ATTN: Rev & Tng Lit Div Fort Bragg, NC 28307
1	Commander US Army Foreign Science & Technology Center ATTN: AMXST-MC-3 2200 Seventh St., NE Charlottesville, VA 22901-5396
1	Commander US Army Belvoir Research and Development Center ATTN: STRBE-WC Fort Belvoir, VA 22060-5606
1	President US Army Artillery Board Fort Sill, OK 73503-5600
1	Project Manager US Army Tank-Automotive Command Improved TOW Vehicle ATTN: AMCPM-ITV Warren, MI 48397-5000
1	Project Manager US Army Tank-Automotive Command Fighting Vehicle Systems ATTN: AMCPM-BFVS Warren, MI 48092-2498
1	Commandant US Army Command and General Staff College Fort Leavenworth, KS 66027

No. of Copies	Organization
1	Commander Radford Army Ammunition Plant ATTN: SMCRA-QA/HI LIB Radford, VA 24141-0298
1	Commander US Army Research Office ATTN: Technical Library PO Box 12211 Research Triangle Park, NC 27709-2211
1	Director US Army TRAC-Fort Lee Defense Logistics Studies Fort Lee, VA 23801-6140
3	Commandant US Army Armor School ATTN: ATZK-CD-MS, M. Falkovitch Armor Agency Fort Knox, KY 40121-5215
1	Commander Naval Sea Systems Command ATTN: SEA 62R Washington, DC 20362-5101
1	Commander Naval Air Systems Command ATTN: AIR-954-Technical Library Washington, DC 20360
1	Naval Research Laboratories Technical Library Washington, DC 20375
1	Naval Surface Warfare Center ATTN: Code G33, W. Burrell Dahlgren, VA 22448-5000
1	Commander Naval Surface Warfare Center ATTN: Code G23, D. McClure Dahlgren, VA 22448-5000

No. of Copies	Organization
1	Commander Naval Surface Warfare Center ATTN: J P. Consaga Indian Head, MD 20640-5000
1	Commander Naval Surface Warfare Center ATTN: Code 240, S. Jacobs Silver Spring, MD 20903-5000
1	Commander Naval Sea Systems Command ATTN: SEA 64 Washington, DC 20362-5101
1	Assistant Secretary of the Navy (R, E, and S) ATTN: R. Reichenbach Room 5E787 Pentagon Bldg. Washington, DC 20375
1	Commander Naval Surface Warfare Center ATTN: Code G33, J. L. East Dahlgren, VA 22448-5000
1	Commander Naval Surface Warfare Center ATTN: Code G33, J. Johndrow Dahlgren, VA 22448-5000
1	Commander Naval Surface Warfare Center ATTN: Code DX-21 Technical Library Dahlgren, VA 22448-5000
1	Commander Naval Surface Warfare Center ATTN: C. Gotzmer Indian Head, MD 20640-5000
1	Commander Naval Surface Warfare Center ATTN: Code 730 Silver Spring, MD 20903-5000

No. of Copies	Organization
1	Commander Naval Surface Warfare Center ATTN: Cord R-13, K. Kim Silver Spring, MD 20903-5000
1	Commanding Officer Naval Underwater Systems Center ATTN: Code 5B331, R. Lazar Newport, RI 02840
1	Commander Naval Weapons Center ATTN: Code 388, C. F. Price Information Science Division China Lake, CA 93555-6001
1	Commander Naval Ordnance Station ATTN: L. Torreyson Indian Head, MD 20640-5000
1	Commander Naval Ordnance Station ATTN: D. Brooks Indian Head, MD 20640-5000
1	Commander Naval Surface Warfare Center ATTN: R. Bernecker Silver Spring, MD 20903-5000
1	Commanding Officer Naval Underwater Systems Center ATTN: Technical Library Newport, RI 02840
1	Commandant US Army Field Artillery Center and School ATTN: ATSF-CO-MW, B. Willis Fort Sill, OK 73503-5600
1	Commander Naval Ordnance Station ATTN: J. Birkett Indian Head, MD 20640-5000

No. of
Copies Organization

1 Commander
Naval Ordnance Station
ATTN: T. C. Smith
Indian Head, MD 20640-5000

1 Commander
Naval Ordnance Station
ATTN: Technical Library
Indian Head, MD 20640-5000

3 AL/LSCF
ATTN: J. Levine
L. Quinn
T. Edwards
Edwards AFB, CA 93523-5000

1 AL/TSTL (Technical Library)
ATTN: J. Lamb
Edwards AFB, CA 93523-5000

1 AFATL/DLXP
Eglin AFB, FL 32542-5000

1 NASA/Lyndon B. Johnson Space Center
ATTN: NHS-22, Library Section
Houston, TX 77054

1 AAI Corporation
ATTN: J. Frankle
PO Box 126
Hunt Valley, MD 21030-0126

1 OSD/SDIO/IST
ATTN: L. H. Caveny
Pentagon
Washington, DC 20301-7100

10 Central Intelligence Agency
Office of Central Reference
Dissemination Branch
Room GE-47 HQS
Washington, DC 20505

1 AFATL/DLYV
Eglin AFB, FL 32542-5000

1 AFATL/DLJE
Eglin AFB, FL 32542-5000

No. of
Copies Organization

1 AFELM, The Rand Corporation
ATTN: Library D
1700 Main Street
Santa Monica, CA 90401-3297

1 Aerojet General Corporation
ATTN: D. Thatcher
PO Box 296
Azusa, CA 91702

2 Calspan Corporation
ATTN: C. Murphy
PO Box 400
Buffalo, NY 14225-0400

1 IITRI
ATTN: M. J. Klein
10 W. 35th Street
Chicago, IL 60616-3799

1 Hercules, Inc.
Allegheny Ballistics Laboratory
ATTN: William B. Walkup
PO Box 210
Rocket Center, WV 26726

1 Atlantic Research Corporation
ATTN: M. K. King
5390 Cherokee Ave.
Alexandria, VA 22312-2302

1 Lawrence Livermore National Laboratory
ATTN: L-355, A. Buckingham
PO Box 808
Livermore, CA 94550-0622

1 Lawrence Livermore National Laboratory
ATTN: L-324, M. Constantino
PO Box 808
Livermore, CA 94550-0622

1 Olin Ordnance
V. McDonald, Library
PO Box 222
St. Marks, FL 32355-0222

No. of Copies	Organization
1	Hercules, Inc. Radford Army Ammunition Plant ATTN: J. Pierce Radford, VA 24141-0299
1	Hercules Incorporated ATTN: R. V. Cartwright Howard Blvd. Kenvil, NJ 07847
1	Aerojet Solid Propulsion Co. ATTN: P. Micheli Sacramento, CA 96813
1	Honeywell, Inc. ATTN: C. Hargraves 7225 Northland Drive Minneapolis, MN 55436
1	Lawrence Livermore National Laboratory ATTN: L-355, M. Finger PO Box 808 Livermore, CA 94550-0622
1	Olin Corporation Badger Army Ammunition Plant ATTN: F. E. Wolf Baraboo, WI 53913
1	Paul Gough Associates, Inc. ATTN: Dr. Paul S. Gough 1048 South Street Portsmouth, NH 03801-5423
1	AVCO Everett Rsch Lab ATTN: D. Stickler 2385 Revere Beach Parkway Everett, MA 02149-5936
1	Princeton Combustion Research Laboratories, Inc. ATTN: M. Summerfield 475 US Highway One Monmouth Junction, NJ 08852-9650
1	Science Applications, Inc. ATTN: R. B. Edelman 23146 Cumorah Crest Drive Woodland Hills, CA 91364-3710

No. of Copies	Organization
1	Thiokol Corporation Huntsville Division ATTN: D. Flanigan Huntsville, AL 35807-7501
1	Thiokol Corporation Huntsville Division ATTN: Technical Library Huntsville, AL 35807-7501
1	Veritay Technology, Inc. ATTN: E. Fisher 4845 Millersport Highway PO Box 305 East Amherst, NY 14051-0305
1	Physics International Company ATTN: H. Wayne Wampler 2700 Merced Street San Leandro, CA 94577-5602
1	Universal Propulsion Company ATTN: H. J. McSpadden Black Canyon Stage 1 Box 1140 Phoenix, AZ 84029
1	Rockwell International Rocketdyne Division ATTN: BA08, J. E. Flanagan 6633 Canoga Ave. Canoga Park, CA 91303-2703
1	Rockwell International Rocketdyne Division ATTN: BA08, J. Gray 6633 Canoga Ave. Canoga Park, CA 91303-2703
1	Morton Thiokol, Inc. Huntsville Division ATTN: Dr. John Deur Huntsville, AL 35807-7501
1	Scientific Research Assoc., Inc. ATTN: H. McDonald PO Box 498 Glastonbury, CT 06033-0498

No. of
Copies Organization

1 Physics International Company
ATTN: Library
2700 Merced Street
San Leandro, CA 94577-5602

1 United Technologies Corp.
Chemical Systems Division
ATTN: Technical Library
PO Box 49028
San Jose, CA 95161-9028

1 Battelle Memorial Institute
ATTN: Technical Library
505 King Avenue
Columbus, OH 43201-2693

1 Brigham Young University
Dept. of Chemical Engineering
ATTN: M. Beckstead
Provo, UT 84601

1 Thiokol Corporation
Elkton Division
ATTN: R. Biddle
PO Box 241
Elkton, MD 21921-0241

1 University of Massachusetts
Dept. of Mechanical
Engineering
ATTN: K. Jakus
Amherst, MA 01002-0014

1 Georgia Institute of Technology
School of Aerospace Eng.
ATTN: E. Price
Atlanta, GA 30332

1 Institute of Gas Technology
ATTN: D. Gidaspow
3424 S. State Street
Chicago, IL 60616-3896

1 California Institute of Technology
Jet Propulsion Laboratory
ATTN: L. D. Strand, MS 512/102
4800 Oak Grove Drive
Pasadena, CA 91109-8099

No. of
Copies Organization

1 California Institute of Technology
204 Karman Lab
Main Stop 301-46
ATTN: F. E. C. Culick
1201 E. California Street
Pasadena, CA 91109

1 Thiokol Corporation
Elkton Division
ATTN: Technical Library
PO Box 241
Elkton, MD 21921-0241

1 University of Minnesota
Dept. of Mechanical Engineering
ATTN: E. Fletcher
Minneapolis, MN 55414-3368

1 Georgia Institute of Technology
School of Aerospace Eng.
ATTN: B. T. Zinn
Atlanta, GA 30332

1 Georgia Institute of Technology
School of Aerospace Eng.
ATTN: W. C. Strahle
Atlanta, GA 30332

1 Johns Hopkins University
Applied Physics Laboratory
Chemical Propulsion
Information Agency
ATTN: T. Christian
Johns Hopkins Road
Laurel, MD 20707-0690

1 Vanderbilt University
Mechanical Engineering
ATTN: A. M. Mellor
Box 6019, Station B
Nashville, TN 37235

1 University of Illinois
Dept. of Mechanical/Industrial
Engineering
ATTN: H. Krier
144 MEB; 1206 N. Green Street
Urbana, IL 61801-2978

No. of
Copies Organization

1 University of Utah
Dept. of Chemical Engineering
ATTN: A. Baer
Salt Lake City, UT 84112-1194

1 Washington State University
Dept. of Mechanical Engineering
ATTN: C. T. Crowe
Pullman, WA 99163-5201

1 Massachusetts Institute of Technology
Dept. of Mechanical Engineering
ATTN: T. Toong
77 Massachusetts Ave.
Cambridge, MA 02139-4307

1 Pennsylvania State University
Dept. of Mechanical Engineering
ATTN: K. Kuo
University Park, PA 16902-7501

1 SRI International
Propulsion Sciences Division
ATTN: Technical Library
333 Ravenwood Ave.
Menlo Park, CA 94025-3493

1 Rutgers University
Dept. of Mechanical and Aerospace Engineering
ATTN: S. Temkin
University Heights Campus
New Brunswick, NJ 08903

1 University of Southern California
Mechanical Engineering Dept.
ATTN: OHE200, M. Gerstein
Los Angeles, CA 90089-5199

1 University of Utah
Dept. of Chemical Engineering
ATTN: G. Flandro
Salt Lake City, UT 84112-1194

No. of
Copies Organization

1 Rensselaer Polytechnica Inst.
Department of Mathematics
Troy, NY 12181

1 Pennsylvania State University
Applied Research Laboratory
ATTN: G. M. Faeth
University Park, PA 16802-7501

1 Purdue University
School of Mechanical Engineering
ATTN: J. R. Osborn
TSPC Chaffee Hall
West Lafayette, IN 47907-1199

1 Stevens Institute of Technology
Davidson Laboratory
ATTN: R. McAlevy, III
Castle Point Station
Hoboken, NJ 07030-5907

1 Honeywell Inc.
ATTN: R. E. Tompkins
MN38-3300
10400 Yellow Circle Drive
Minnetonka, MN 55343

Aberdeen Proving Ground

Dir, USAMSAA
ATTN: AMXSY-GI, CPT Klimack

INTENTIONALLY LEFT BLANK.

USER EVALUATION SHEET/CHANGE OF ADDRESS

This Laboratory undertakes a continuing effort to improve the quality of the reports it publishes. Your comments/answers to the items/questions below will aid us in our efforts.

1. BRL Report Number BRL-TR-3181 Date of Report JANUARY 1991

2. Date Report Received _____

3. Does this report satisfy a need? (Comment on purpose, related project, or other area of interest for which the report will be used.) _____

4. Specifically, how is the report being used? (Information source, design data, procedure, source of ideas, etc.) _____

5. Has the information in this report led to any quantitative savings as far as man-hours or dollars saved, operating costs avoided, or efficiencies achieved, etc? If so, please elaborate. _____

6. General Comments. What do you think should be changed to improve future reports? (Indicate changes to organization, technical content, format, etc.) _____

CURRENT ADDRESS

Name

Organization

Address

City, State, Zip Code

7. If indicating a Change of Address or Address Correction, please provide the New or Correct Address in Block 6 above and the Old or Incorrect address below.

OLD ADDRESS

Name

Organization

Address

City, State, Zip Code

(Remove this sheet, fold as indicated, staple or tape closed, and mail.)